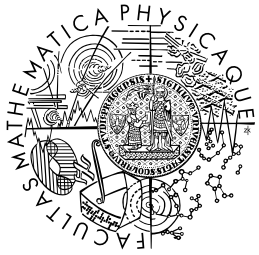

FACULTY
OF MATHEMATICS
AND PHYSICS
Charles University

MASTER THESIS

Jiří Doležal

Modification of silicon surfaces for selective adsorption

Department of Surface and Plasma Science

Supervisor of the master thesis:	Doc. RNDr. Ivan Ošťádal, CSc.
Study programme:	Physics
Study branch:	Physics of Surfaces and Ionized Media

Prague 2018

I declare that I carried out this master thesis independently, and only with the cited sources, literature and other professional sources.

I understand that my work relates to the rights and obligations under the Act No. 121/2000 Sb., the Copyright Act, as amended, in particular the fact that the Charles University has the right to conclude a license agreement on the use of this work as a school work pursuant to Section 60 subsection 1 of the Copyright Act.

In ..... date ..... signature of the author

Title: Modification of silicon surfaces for selective adsorption

Author: Jiří Doležal

Department: Department of Surface and Plasma Science

Supervisor: Doc. RNDr. Ivan Ošťádal, CSc., Department of Surface and Plasma Science

Abstract: This thesis is focused on adsorption of phthalocyanines on tin and indium passivated silicon Si(111) surfaces with the $\sqrt{3} \times \sqrt{3}$ reconstruction at room temperature. Scanning tunneling microscopy was used for obtaining atomically resolved surface images. Molecules on these surfaces predominantly adsorb on Si-substitutional defects. Local density of states (LDOS) of strongly adsorbed molecules was obtained by scanning tunneling spectroscopy. The origin of fuzzy imaging of molecules sitting on Si-substitutional double defects was probed. Voltage dependence of mean lifetime of two observed states, between which the "fuzzy" molecule is switching, was measured by analysis of tunneling current fluctuations. We discussed the influence of external parameters on the switching between the two states. We attribute the fuzzy behaviour of the molecule and resulting tunneling current fluctuations to the motion of the molecule in a double-well potential and propose two most likely kinds of the motion which most closely agree with the obtained data.

Keywords: STM, phthalocyanine, Si(111), STS, tin

My biggest gratitude goes to my supervisor Ivan Ošťádal for his guidance throughout my master studies, critical view on the experiments and time spent on discussing and correcting my thesis.

I would also like to thank other members of the Thin Films group, namely Pavel Sobotík and Pavel Kocán for helping me with the experiments and Karel Majer for discussing the time series analysis.

Last but not least, special thanks go to my family and girlfriend Michaela not only for their never-ending support but also for the grammar corrections of the thesis which provided my brother Petr, undergraduate physics student at the University of Cambridge.

Contents

Introduction

Electronics is today based mainly on semiconductor technology. Semiconducting devices represented by transistors are being scaled down following the well known empirical Moore's law, which states that the number of transistors in a dense integrated circuit doubles about every two years. This is possible due to the lithographically created circuits and ion dopant implementation that enable us to create PN junction with size of tens of nanometers. Hand in hand with the miniaturization, the computational power per area of chip increases and enables to use e. g. smartphones with parameters of the best personal computers decade ago. However, further miniaturization will approach its physical limit in near future. Both quantum effects and poor heat dissipation are problems occurring at the nanoscale that cannot be overcome and if we want to push the size of devices further down, different technology should be developed.

Molecules are ideal building blocks in so called bottom up assembly. They are well defined, with various properties and dimensions in the range of few nanometers and they tend to self-organize on certain surfaces. Moreover, chemical reaction of molecules on surfaces induced e. g. by heat [1] or light can create large connected chemical structures. Molecular scale electronics, that employ functionalized molecules or groups of molecules as small integrated circuits, could be the successor of conventional semiconductor electronics. To be so, three main tasks have to be fulfilled. Firstly, we have to create functional molecules that behave like wires, switches, sensors diodes and transistors. A promising progress has been shown so far e. g. on switches [2]. Secondly, these functional blocks have to be fabricated in millions, redistributed on surface and connected in an appropriate way. This is very challenging task since with the help of self-assembly we can theoretically create large arrays, but the conductivity between each block is poor because self-assembly is accompanied with Van der Walls bonding rather than covalent one, which has much better electron transport properties. A novel approach was demonstrated by Grill et al. [1], who first grew self-organized array and then covalently connected neighbouring molecules by subsequent heating. Third major problem today is contacting the molecules to the electrodes and creating so small electrodes. Even though the molecular transport requires lower voltages and much lower currents (few electrons instead of mA in semiconductor technology) and therefore their favourable power consumption could be a big advantage of molecular scale electronics, the instability of molecules due to their high sensitivity to the local environment can make the operation of such device impossible [2]. It is expected that most of the parts of a chip will still be based on semiconductors in future but molecular electronics devices can complement silicon-based devices, add new functionalities and the silicon-based devices would be combined with molecular building blocks on them [3]. Passivation of silicon surfaces and the growth of molecules on them is therefore of general interest.

The topic of this thesis is part of a fundamental research of the molecule growth on passivated silicon surfaces in the Thin Films group at the Department of Surface and Plasma Science. Phtalocyanines were used due to their high thermal stability in ulta-high vacuum (UHV), ease of sublimation and small flat size which make them suitable candidates to study using room temperature scanning

tunneling microscopy (STM). As it often turns out the new physical effects have been discovered unexpectedly in the course of other studies. The research of molecules on the nanoscale could have far-reaching success in all kinds of natural sciences as chemistry, biology, medicine, drug delivery etc..

Aims of the thesis

This thesis deals with experimental study of adsorption of phthalocyanines on passivated silicon surfaces – Si(111) by tin and indium. Special interest is given to unravel the origin of "fuzzy" imaged phthalocyanines on adsorbed on Si-substitutional double-defects on the Sn/Si(111)–($\sqrt{3} \times \sqrt{3}$) R30° reconstruction. All experiments were done using STM and associate methods: Scanning tunneling spectroscopy (STS) and analysis of tunneling current fluctuations. The aims of the thesis as defined by the Charles University are as follows:

1. Selection of appropriate surfaces for experimental study based on the already studied Si-metal (especially In and Sn) surfaces in the literature.

2. Preparation of surfaces with defined amount of defects.

3. Measurement of the morphology and electron structure of selected surfaces in STM.

4. Deposition of phthalocyanine molecules at low coverage in order to study adsorption of individual molecules.

5. Creation of surfaces with larger coverage of molecules and study their interaction.

1. Scanning tunneling microscopy

1.1 History of STM

First successful attempt to construct a scanning probe microscope using a tip as a probe was done by Russel D. Young who constructed the Topografiner in 1971 [4]. The Topografiner is a forerunner of the today's STM. The principle of its work is similar to STM, it employs field emission current between two electrodes – metal tip and the conductive sample – as a feedback signal instead of the tunneling current in STM. The tip-sample distance d in topografiner is 100 nm, much more than it is in STM, disabling the atomic resolution. Unfortunately, smaller separation distance was impossible to achieve since the vibration stabilization of the system was poor even though Young knew that operation in a tunneling mode would provide atomic resolution. The ultimate resolution of the Topografiner was estimated to 0.3 nm in vertical direction, limited by the noise, and 20 nm in the lateral direction limited by the tip radius. It is worth to mention that the first atomic resolution was obtained by field ion microscope in 1956 [5] but it projected only the sample in a shape of a sharp tip – the atomic planes in the very end of it. In 1981 G. Binning and H. Rohrer, researchers in IBM Zürich, constructed the first STM operating in the tunneling regime. Improvement of the vibration isolation and the feedback control made possible to resolve individual atoms on surfaces. Real space atomic resolution of the Si(111)-(7 × 7), very intriguing problem of surface science, made STM very famous. In 1986, Binnig and Rohrer have been awarded the Nobel prize in physics for invention of the STM.

1.2 Tunneling effect

STM could not work without the tunneling effect. Tunneling is a manifestation of quantum nature of particles already known from 1920s. In classical physics, particle that has lower energy than the energy of a barrier cannot surmount it, while in quantum physics, there is a non-zero probability that the particle will tunnel through. In we consider the simplest case, 1D barrier of rectangular shape depicted in Fig. 1.1 of height W and width d and a particle of energy E and mass m, the probability P for the particle to traverse the barrier is given by

$$P \propto e^{-2kd} \tag{1.1}$$

where

$$k = \sqrt{\frac{8\pi^2 m(W-E)}{h^2}} \tag{1.2}$$

and h is the Planck constant [6]

1.3 Principle of STM

The STM apparatus consists of a sharp tip and a conductive sample separated approximately 0.5 nm. Applying the voltage between the tip and the sample causes

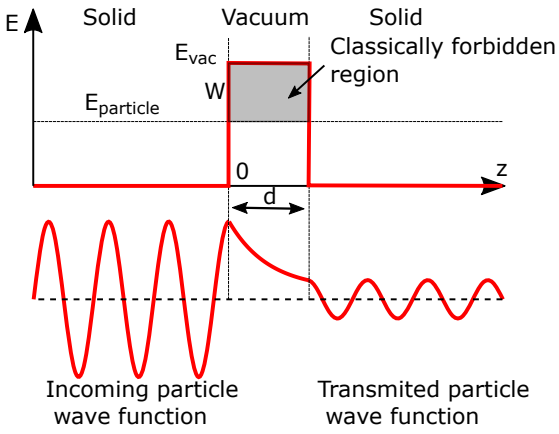

Figure 1.1: Illustration of electron tunneling through a 1D barrier of height W and width d. The upper graph shows the potential for a solid-vacuum-solid configuration, where vacuum is the barrier. The lower graph shows the real part of the electron wave function oscillating in front of the barrier, exponentially decaying inside the barrier and again oscillating past the barrier.

change in the mutual energy levels of both electrodes and a tunneling of electrons through the barrier from the occupied states of negatively biased electrode to the unoccupied states of positively biased electrode. The tip is scanning along the surface and the value of tunneling current, position of the tip and other parameters are recorded. For low voltages V_{T} and low temperatures we the tunneling current behaves as [6]

$$I \approx 18 \frac{V_{\mathrm{T}} k}{10^4 \Omega d} A_{\mathrm{eff}} e^{-2kd} \tag{1.3}$$

where $2k\ [\mathrm{\AA}^{-1}] = 1.025\sqrt{W}\ [\mathrm{eV}]$, W is the average work function, assumed equal to the mean barrier height between the two electrodes. A_{eff} is the typical effective area involved in tunneling determining the lateral resolution, d is the tip sample separation and Ω is the Ohm unit. Plugging typical $W = 5$ eV for metals in equation 1.3 we find the change of the tunneling current I by one order of magnitude for the 1 Å change in he distance. This means that the tip does not need to be macroscopically sharp for gaining the atomic resolution. It is sufficient for scanning on flat samples if the end of the tip is formed by a cluster of atoms where more than 70% of tunneling current flows through.

There are two basic modes of operation of the STM. Constant current mode and constant height mode. **Constant current mode** is the most frequently used one. The tunneling current is held constant by a feedback loop. In the case of an electronically homogeneous surface, constant current means constant separation d and the tip movement in the piezoceramics coordinate system corresponds to the topography. The biggest advantage of this mode is that it can be used on surfaces with various roughness without destroying the tip.

In the **constant height mode** the tip can scan rapidly across the surface, which is the main advantage. Assuming the typical tip sample distance of 0.5 nm, the surface roughness of scanned area must be within that range in order to avoid crashing the tip. Furthermore, the value of work function must be known, if the z scale has to be calibrated properly. In practice, constant height mode is not used very often – mainly on small areas if e. g. dynamics on the surface is the

object of our interest.

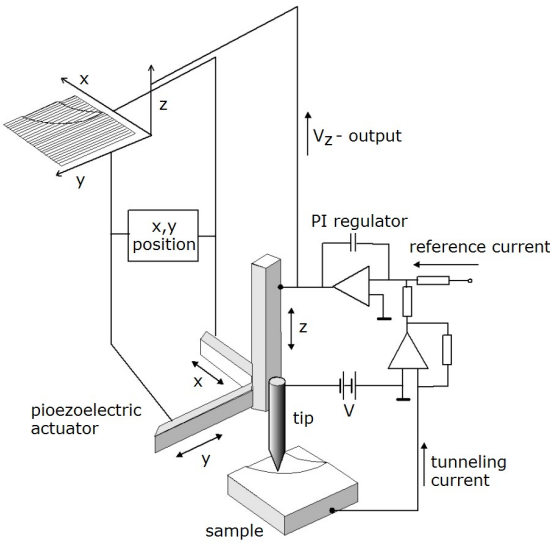

Figure 1.2: Schematic view of the STM. Tunneling current flows in a feedback loop which adjusts the z position of the tip. z as a function of x and y is plotted. Adapted from a Thin Films group archive.

1.4 Theory of tunneling

First analytical approach to tunneling is the Bardeen model which was introduced before inventing the STM in 1961 for metal-insulator-metal heterostructures [7]. This model considers tip plus barrier and a sample plus barrier as two separate systems. Specific theoretical approaches differ from each other in the wavefunctions of each electrode used. The wavefunctions of these two systems can be approximated as in the case of the 1D barrier depicted in Fig. 1.1, or in the 3D model, but they are more complicated taking the geometry of spherical symmetric tip and flat sample into account. Transition rate from one electrode to another is calculated using time-dependent perturbation theory and the tunneling current is proportional to the rate.

General equation for the tunneling current in the low temperature limit can be written as

$$I = \frac{8\pi^2 e}{h} \sum_{i,f} |M_{fi}|^2 \delta(E_f - E_i) \tag{1.4}$$

where we sum over all combinations of initial states and final states of electrons both for the tip and the sample in the applied bias window. $\delta(E_f - E_i)$ denotes that the tunneling can occur only on the same energy levels. $|M_{fi}|$ is a matrix element which denotes the probability of an electron passing the barrier and depends on ψ_i and ψ_f as well as on the shape of the barrier [8].

Two kinds of approximation of the Bardeen's equation (1.4) are most widespread. In the **Tersoff-Hamann** approximation the applied voltage bias between the tip and the sample is considered to be small in comparison with the barrier height. Energy dependence of the the matrix element and energy dependence of

the densities of states is neglected. The tip wave function is approximated by a spherical s-wave. This approximation is often used for simulation of STM images.

Energy-dependent approximation deals with a 1D barrier approximation of a rectangular shape but takes into account energy dependence of densities of states of the tip and the sample. With this approximation we are able to derive important equations used in scanning tunneling spectroscopy (STS). Again, in the low temperature limit, tunneling current can be approximated as

$$I(V,d) = \frac{8\pi^2 e}{h} \int_0^{eV} \rho_{\text{tip}}(\varepsilon - eV)\rho_{\text{sample}}(\varepsilon)T(\varepsilon,V,d)d\varepsilon \tag{1.5}$$

where ε is an energy relative to the Fermi energy of the sample depicted in Fig. 1.3, V the applied bias voltage to the sample, ρ_{tip} and ρ_{sample} are densities of states of the tip and the sample respectively and $T(\varepsilon,V,d)$ is the transmission factor given by

$$T(\varepsilon,V,d) \propto \exp\left[-2d\sqrt{\frac{8\pi^2 m}{h^2}\left(\frac{\Phi_{\text{tip}}+\Phi_{\text{sample}}}{2}+\frac{eV}{2}-\varepsilon\right)}\right] \tag{1.6}$$

where m is the mass of the electron, Φ_{tip} and Φ_{sample} work functions of the tip and the sample respectively. For low bias voltages, the equation 1.5 can be further simplified if we neglect the energy and voltage dependence of T and remove it from the integral.

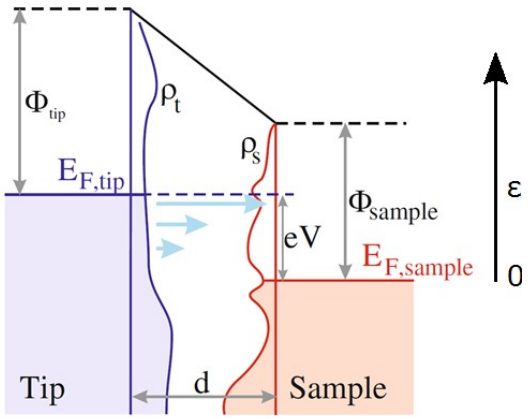

Figure 1.3: Energy level diagram of the tunneling junction. The applied bias shifts the Fermi level by eV . Density of states are represented by ρ_{tip} and ρ_{sample} (the filled states are coloured). Reprinted from [8].

1.5 Construction of the STM

Even though the principle of the STM operation is clear and it might seem that one can measure with a sharp tip in the constant current mode forever, the reality is completely different. First of all, making the STM successfully operational is a demanding process and in 1990s, when commercial STM was not available, only few research groups in the World were able to construct a working apparatus. Furthermore, obtaining and maintaining the atomic resolution is a process that requires a lot of care. In the following, the crucial elements of the STM and the best practice to obtain atomic resolution will be described.

1.5.1 Piezoelectric actuators

For operating the STM, there is a requirement on the resolution of the tip position change – 0.1 nm in the horizontal direction and 0.01 nm in the vertical direction. This is possible if we use piezoceramic material. These materials change their shape in the presence of an external electric field. We can apply the voltage between the electrodes of the actuator in the range of hundreds of Volts in both polarities with a millivolt precision. The piezo actuator is deformed in a way that the tip mounted on it can move with the desired resolution.

The tube piezo element from the $Pb(Ti.Zr)O_3$ (PZT) material is the most widely used actuator [8]. Schematic view of the piezo tube is depicted in Fig. 1.4. Its main advantages are low crosstalk of the electrodes, high resonance frequency and high piezoelectric constants [8]. The common drawbacks of piezoceramics are non-linearity, hysteresis and creep. Non-linearity of the movement of the element on the electric field can be suppressed by limiting the maximal value of applied electric field. Hysteresis will not be visible in the image if the tip scans only in one direction. Creep is the most common effect that appears in an STM image – the topography is deformed. In case of the rapid voltage change, the position change of the ceramics holding the tip does not change instantaneously, but rather with a delay in order of seconds or even minutes (function of logarithm of time). One has to wait sufficient time until the creep is negligible and does not "travel" with the tip on long distances in a short time.

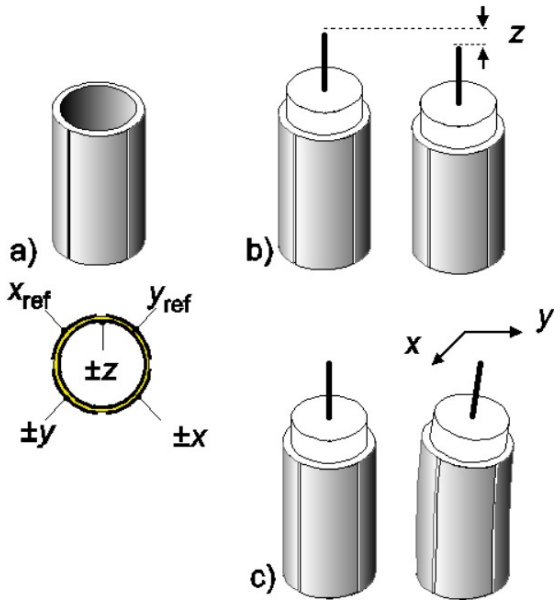

Figure 1.4: Tube piezoelectric actuator. a) Schematic diagram of the connection of the electrodes on the tube. b) Contraction of the tube in the vertical direction along z induced by applied voltage on z electrode. c) Combination of electric field in the x and y direction causes tilting of the tube and enables scanning of the mounted tip. Taken after doc. Ivan Ošťádal.

1.5.2 Tip

Tip is the heart of the STM. If we have the STM head protected from external vibrations and electrical noise the STM image is a result of the tip quality only. The tip has to be sharp and conductive – metallic – without any impurities and stable. Ideally, the macroscopically sharp tip should be terminated with cluster of atoms and the tunnelling current should flow between the last atom and the sample only. The sharpness of the tip is important for the in-vivo measurement where the deposition of adsorbates happens simultaneously with scanning and the tip must not shade the molecular beam. If there are more clusters on the tip, the image is multipled as it is most prominent on steps and islands — the resulting profile of the tip motion is given by the geometrical convolution of the tip cross-section and the sample profile.

If the tip gets blunt during the measurement there are many ways how to reshape it. Basic operations are voltage pulses and a controlled approach of the tip towards the surface. Atoms on the apex might rearrange themselves through the influence of a strong electric field or through pressing the tip in the sample, when atoms from the sample can be grabbed. The best operation depends mainly on the surface. Another widely used technique is an exchange of the samples and scanning and crashing the tip on the platinum crystal. This makes the tip metallic again. If the tip is not sharp at all, bringing the tip to the contact with a tungsten metal sheet and the subsequent annealing of the tungsten causes melting of the apex of the tip together with the metal sheet. When we retract the tip, a brand new clean tungsten apex is created. The tip is not macroscopically sharp but this is not usually a problem for obtaining the atomic resolution.

1.5.3 Vibration isolation

A typical tip-sample distance d is 0.5 nm and the fluctuation of this distance caused by vibrations must be at least three orders of magnitude lower in order to have high quality images. Vibration isolation system consists of a rigid tip-sample mechanical loop with high resonance frequency and springs on which an STM head hangs with low resonance frequency and eddy current damping. Whole apparatus stands on pneumatic isolation legs that also have low resonance frequency (1–2 Hz). High frequencies are damped with low resonance frequency elements and vice versa. An STM is therefore most susceptible to frequencies in the region between 1–100 Hz. These are caused by building vibrations, acoustic noise or walking around apparatus. Hence, an STM is usually located in the ground floor.

1.6 Scanning tunneling spectroscopy

As the equation 1.5 states apart from the distance dependence the tunneling current is proportional to the density of states of the tip and the sample. If we consider constant density of states at the tip – taken independent on the energy (which is not completely valid for tungsten, but often done) – the first derivative

of the tunneling current with respect to the bias voltage is proportional to

$$\frac{dI}{dV} \propto \rho_{\text{sample}}(d, \varepsilon) T(\varepsilon, V, d) \tag{1.7}$$

For most of the surfaces, the transition factor is proportional to the conductance I/V and the so called normalized differential conductance is given by the equation

$$\frac{dI/dV}{I/V} \propto \rho_{\text{sample}} \tag{1.8}$$

The normalized differential conductance can be measured at different positions on the surface and corresponds to the local density of states (LDOS). For some surfaces or objects e. g. molecular layers, normalized dI/dV does not correspond properly to the LDOS and only differential conductance or other types of normalization are used [9]. Scanning tunneling spectroscopy (STS) measurements, obtaining the dI/dV, can be done in two ways. A simple approach is to numerically differentiate the measured $I - V$ characteristics. Unfortunately, numerical differentiation amplifies the noise in the signal. Therefore, synchronous lock-in detection is often used.

1.6.1 Lock-in detection

Lock-in amplifier adds a small modulation voltage $V_M \cos \omega t$ to a bias voltage and this modulation appears in the measured current: $I(t) = f(V + V_M \cos \omega t)$. The modulation frequency f should be higher than the cutoff frequency of the feedback loop (965 Hz in our case) and the modulation voltage has to be as small as possible (50 mV in our case). The phase-shift between the reference modulation signal and the measured signal which emerges due to the parasitic capacitance of the wires (consider a parallel RC circuit) in the STM must be eliminated. In practice, before each STS measurement the tip is slightly retracted out of the contact and only the AC component of the measured current flows through the tunneling junction (the phase shift of the measured current is 90°) and the capacitance can be measured and the phase-shift eliminated with the lock-in amplifier. If we slowly change the voltage during an $I(V)$ measurement, the measured tunneling current can be estimated using Taylor expansion as:

$$I(V + V_M \cos \omega t) \propto I(V) + \frac{dI(V)}{dV} V_M \cos \omega t + \frac{d^2 I(V)}{dV^2} \frac{{V_M}^2}{2} \cos^2 \omega t + ... \tag{1.9}$$

and a trigonometric identity gives us

$$\cos^2 \omega t = \frac{1}{2} + \frac{1}{2} \cos 2\omega t \tag{1.10}$$

We can see that harmonic term with ωt has an amplitude proportional to the first derivative of the tunneling current with respect to the voltage and the term with $2\omega t$ – second harmonic is proportional to $\frac{d^2 I(V)}{dV^2}$. With the help of filters that are implemented in the lock-in amplifier, amplitudes of desired n-th harmonic frequencies are obtained. While in STS we use the first harmonic and the first derivative, the second derivative is used in inelastic tunneling spectroscopy. For

the high quality spectrum each voltage step should last at least 10 periods of modulation.

The energy resolution of the STS spectrum is determined by the thermal broadening of the Fermi level by 3.2 kT and by the instrumental broadening by the modulation voltage. Total error can be calculated as [8]:

$$\Delta E = \sqrt{(2eV_{\mathrm{mod,RMS}})^2 + (0.28\ \mathrm{meV/K} \cdot T)^2} \tag{1.11}$$

At room temperature, the energy resolution is 83 meV, hence it is always beneficial to perform STS at low temperatures.

1.7 Analysis of tunneling current fluctuation

While $I(V)$ characteristics allow us to obtain the LDOS of the surface, $I(t)$ characteristics, analysis of tunneling current fluctuation, gives us information about the dynamics on the surface and changes in the tunneling junction. It was introduced and firstly realized in STM by Wang et al. [10] – he demonstrated its ability to capture fast processes with hopping rate up to 10^4 Hz on diffusion of Cu atoms on Si(111)–(7×7). In an STM image, the objects that move on the surface fast and its residence time in one position is shorter that is the acquisition time of the image appear fuzzy.

Likewise to the $I(V)$ (STS spectra), the tip movement is stopped during scanning (usually in constant current mode) at a desired lateral position and height (determined from the feedback loop which maintains a set tunneling current) and tunneling current is recorded for a given time interval. According to the number of positions of the atom under the tip we see a multiple-level fluctuation of tunneling current. The useful signal is also mixed with noise. Using various methods, the signal can be divided into time intervals t_{ki} where k is the index of the current level and i is the index of a given time interval in the given current level (state). A random process linked with motion of an object on a surface follows Poisson distribution. Now we have sets of N_{k0} discrete residence time values in each state k. We can count discrete cumulative density function (CDF)

$$P_k(t_\mathrm{n}) = N_k(x \leq t_\mathrm{n})/N_{k0} \tag{1.12}$$

which is the probability of residence in a given state in time less or equal than t_n. For Poisson distribution, this continuous function is

$$P_k(x \leq t) = 1 - exp(-t/\tau_k) \tag{1.13}$$

where τ_k is the mean lifetime for state k. By fitting our measured discrete sets of data with this function we obtain mean lifetime of residence in given state and its error. In practice, "survival function" which is the complementary probability to CDF $P_k(x > t) = 1 - P_k(x \leq t)$ is more straightforward to fit since it is given by

$$P_k(x > t) = exp(-t/\tau_k) \tag{1.14}$$

Time series analysis may be applied not only on moving atoms but also on molecules and effects involving change of electronic structure of the molecule. Examples of two state fluctuations and a completely new approach of measuring

time series was shown by Schaffert et al. [11]. He developed a new method called Scanning noise microscopy. In principle, it works like usual STM but it measures time series in each pixel of an image. After that, the amplitude, rate and duty cycle is calculated and spatial resolved maps of these quantities are plotted together with a topography image.

2. Silicon surface

Silicon is an element of IV.A group located in the third period. It crystallizes in face-centered diamond cubic structure depicted in Fig. 2.1. Due to the sp^3 hybridization of orbitals, every silicon atom in bulk crystal forms 4 covalent bonds with its neighbours. Silicon is a semiconductor and the second most abundant element in Earth's crust. It is its availability what made the development of cheap and powerful electronics possible. As a consequence of its usage in electronics, it is one of the most extensively studied elements. Three basic low-index planes can be created by cleaving — Si(111), Si(100), Si(110) — sorted from the most dense packed one to the least dense one. However, when creating the surface we cut the covalent bonds and create unsaturated dangling bonds. The surface in UHV is not stable and tends to reconstruct itself. In our work, we have used only a Si(111) sample hence I will concentrate only on its most favourable reconstruction (7×7).

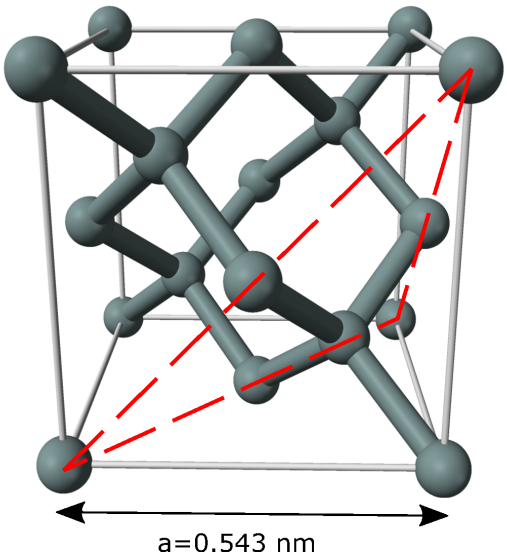

Figure 2.1: Ball-and-stick model of unit cell of silicon crystal. Red dashed lines mark the cut through 111 plane.

2.1 Si(111)–(7×7)

The Si(111)–(7×7) is a very complex surface and resolving its structure is to a large extent attributed to STM. Its structural model, STM imaging and description is in Fig. 2.2. The total number of dangling bonds per area of the (7×7) unit cell is reduced from 49 (1 dangling bond per atom at Si(111) termination) to 19 by this reconstruction and therefore the reconstruction is stable in UHV. This is still a large number and the surface is highly reactive.

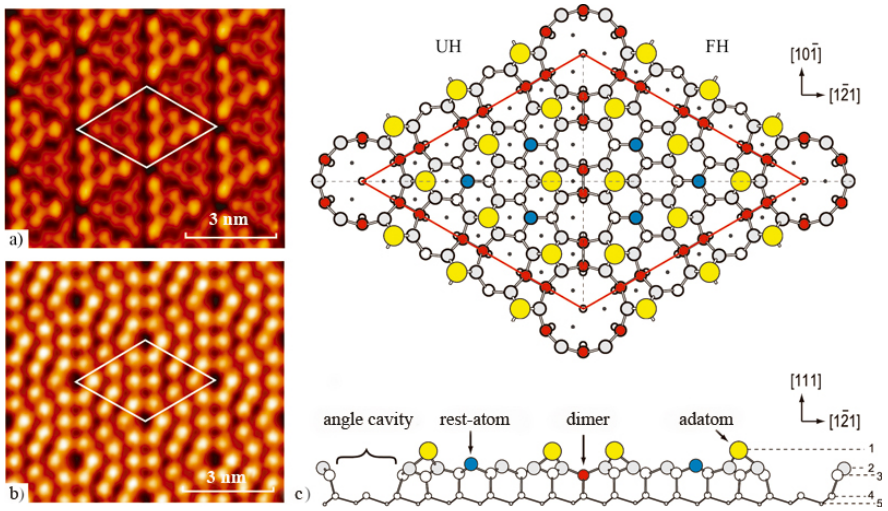

Figure 2.2: Atomically clean surface of Si(111)–(7×7). STM images of (a) filled and (b) empty electron states of surface; (c) Schematic representation of surface (plan and side views) in accordance with Takayanagi DAS model (dimer-adatom-stacking fault) [12]. Yellow circles represent silicon adatoms, red circles silicon atoms forming a dimer, blue circles – second layer Si rest-atoms. In corners of the primitive unit cell (highlighted with red rhombus) are angle cavities – frequently called corner holes. Two parts of the primitive unit cell divided by the axis along dimers are not equivalent. Half of the unit cell with the package defect with respect to the bulk Si is called faulted half and the other half with no package defect is unfaulted half. Faulted half appears brighter in filled state STM image in (a). Bright features (maxima) in empty state STM image in (b) correspond to the adatoms. Taken from [13].

3. Metal adsorbates on Si(111)

3.1 Surface passivation

Surface passivation is a tool, mainly used for semiconductors, for saturating their dangling bonds (DB) and decrease the reactivity of the surface. In semiconductor industry's boom it has became very important and several procedures were developed to passivate silicon surface e.g. second step of RCA cleaning procedure [14], where silicon wafers are immersed in HF solution which leads in DB passivation by hydrogen and prevents recontamination of previously cleaned Si samples. Not only the reactivity is decreased by the passivation, but also the potential energy landscape is smoothed and passivated silicon surfaces have less corrugated potential energy landscape (see Fig. 3.1) but also still more corrugated than e.g. metal surfaces [15]. Surface reactivity and corrugation is a parameter of great importance for self-organizing of molecules and it will be discussed in the next chapter.

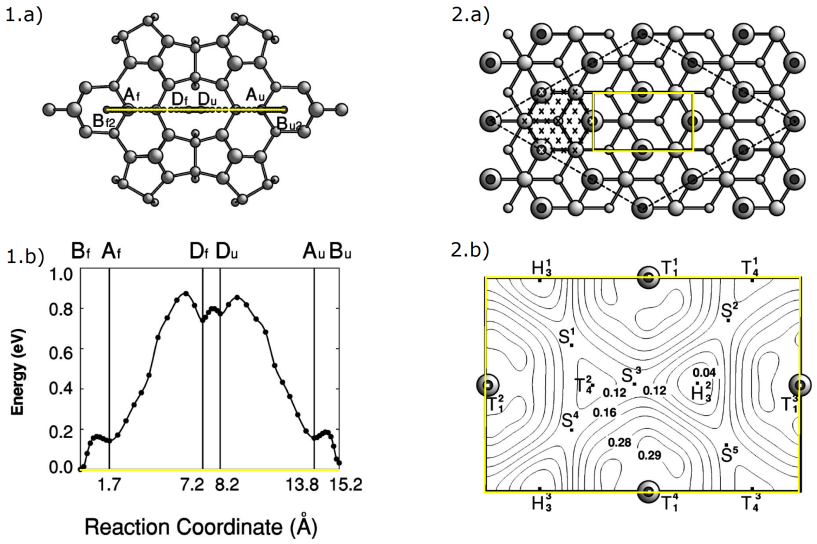

Figure 3.1: Ag diffusion on the clean 7×7 in 1) and H-terminated Si(111) surface in 2). Path in the structural model a) is marked with yellow line and potential energy along it is in b). [16]

One can use other elements to passivate silicon. In our Thin Films group, research of metals from III.A and IV.A on silicon surfaces have been studied for long time, hence the first choice for elements acting as passivating agent was tin and indium.

3.2 Tin on Si(111)

Tin is an element of IV.A group where we can also find famous semiconductors silicon and germanium. It has both metallic and semiconducting allotropes [17].

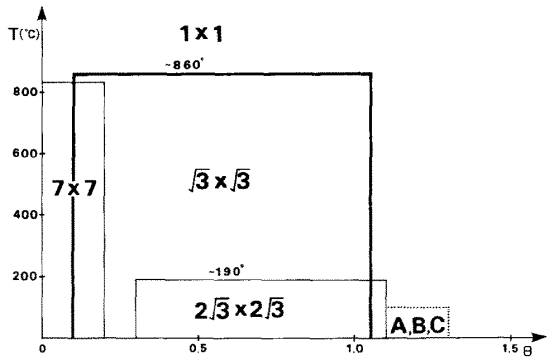

Figure 3.2: Phase diagram of Sn on Si(111). A,B,C are three types of superstructures observed at higher coverages and discussed in text. [19]

Its reconstruction on silicon surface was first studied by Estrup and Morrison [18] in their pioneering LEED (Low energy electron diffraction) study in 1964, two decades before STM was invented. They proposed the $\sqrt{3} \times \sqrt{3}$ reconstruction which exists for many others elements on silicon (B, Ag, Al, In, Tl...). Ichikawa et al. [19] performed phase diagram (Fig. 3.2) using RHEED (Reflection high-energy electron diffraction) and showed coexistence of $\sqrt{3} \times \sqrt{3}$ and $2\sqrt{3} \times 2\sqrt{3}$ reconstructions up to one monolayer (ML) of coverage. The $2\sqrt{3} \times 2\sqrt{3}$ reconstruction turns into $\sqrt{3} \times \sqrt{3}$ when annealed above around 190 °C[20]. For coverages higher than 1 ML, three other more complicated reconstructions were observed ($\sqrt{133} \times 4\sqrt{3}$, $3\sqrt{7} \times 3\sqrt{7}$ R$(30 \pm 10.9)°$, $2\sqrt{91} \times 2\sqrt{91}$ R$(30 \pm 3)°$ – A,B,C in fig. 3.2). Törnevik et al. [21] observed that after further annealing, tin atoms start to desorb and are mostly replaced by silicon atoms. At circa 850 °C, almost half of the tin atoms is replaced by silicon forming so called "mosaic" [21] or γ [22] phase with coverage 1/6 ML. Over 850 °C, areas with clean Si(7×7) appear and at 950 °C all tin atoms are desorbed. Since most of our work has been done on the Sn/Si(111)–$(\sqrt{3} \times \sqrt{3})$ R30° I will discuss this surface more in detail.

3.2.1 Sn/Si(111)–$(\sqrt{3}\times\sqrt{3})$ R30°

The structural model of $\sqrt{3}\times\sqrt{3}$ – hereafter $\sqrt{3}$ – ideal (defect-free) reconstruction is depicted in figure 3.3. In STM images Sn atoms appear as bright protrusions in both empty and filled states. Until 2007 the surface was expected to be metallic or small gap semiconductor (according to STS taken at room temperature [22]), but in 2007 Modesti et al. [23] confirmed theoretical expectations [24] and showed that this surface has an insulating ground state under 70 K.

Whereas defects on surfaces are usually considered problematic and one tries to avoid them when preparing the surface (by means of low pressure and long annealing), in the case of this surface, they attracted much attention due to their potential influence on an expected low temperature phase transition ($\sqrt{3}\times\sqrt{3} \rightarrow 3 \times 3$) [25]. This transition was previously observed on Sn/Ge(111) [26] but until now no significant evidence of non-local phase transition on Sn/Si(111) has been gathered. Generally, 3 types of defects occur on the $\sqrt{3}$ reconstruction [27, 28] – Si-substitutional defects (S), vacancies (V) and Sb (dopant of silicon samples) defects (D), see Fig. 3.4. Vacancies always look like dark holes in both the empty

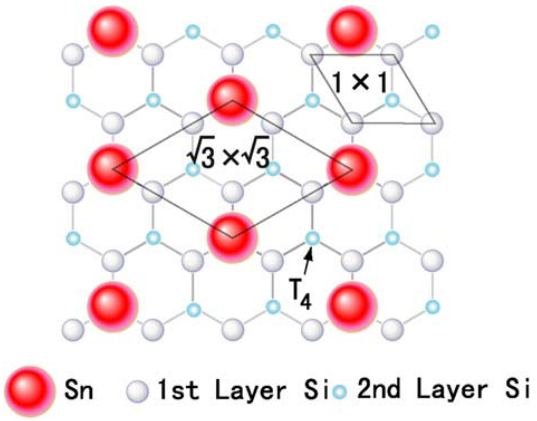

Figure 3.3: Structural model of the Sn/Si(111)–($\sqrt{3}\times\sqrt{3}$) R30°. Tin atoms sit in the T_4 position – on top of the silicon atoms in the 1st layer. [25]

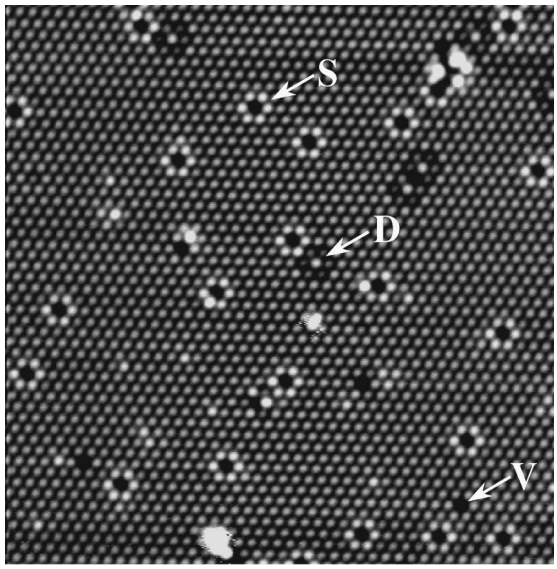

Figure 3.4: 3 basic types of defects on the Sn/Si(111) $\sqrt{3}$ surface. Filled state image with $U_s = -1$ V. Substitutional Si atoms (S), Sb substitutional atoms (D) and vacancies (V) are labelled with arrows. [25]

and filled state STM image. Substitutional defects are dark in filled state image and have characteristic bright neighbourhood – 6 first neighbouring Sn atoms show up with increased hight down to a bias of 10 mV [29]. In empty states, with sample bias between 1 V to 1.5 V, silicon atoms are almost as bright as Sn ones, but with the voltage further increased, they look dark again. The third type of defect is observed on samples doped by Sb. In filled states (sample bias -1 V) it appears as a bright spot with dark nearest neighbours – opposite to Si-substitutional defect, and at smaller negative, or positive sample bias they look dark.

3.2.2 Sn/Si(111)–($2\sqrt{3}\times 2\sqrt{3}$) R30°

The Sn/Si(111)–($2\sqrt{3}\times 2\sqrt{3}$) R30° – hereafter $2\sqrt{3}$ – reconstruction occurs when substantially larger amount of tin is deposited. Mostly, it coexist with $\sqrt{3}$ and,

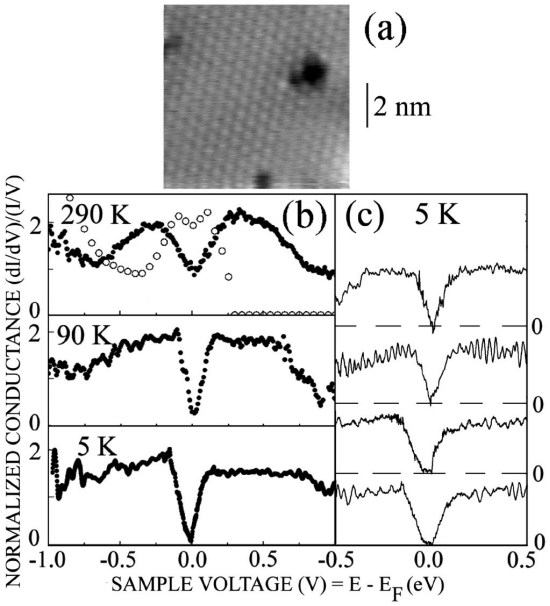

Figure 3.5: (a) Filled states STM image of the Sn/Si(111)–($\sqrt{3}\times\sqrt{3}$) R30° at 5 K, sample bias 1.9 V, tunnelling current 0.3 nA. (b) •: average tunnelling spectra of the same surface measured far from the defects at different temperatures, ∘: calculated normalized conductance from [22]. (c) Single conductance spectra at 5 K. [23]

only in a narrow interval between 1.05 and 1.1 ML coverage and under 190 °C, pure $2\sqrt{3}$ can be observed [30]. It is quite difficult to tell its structure based only on STM images. Törnevik [31, 21] tried to do so and proposed a 2-layer model with 4 atoms in a top layer and 10 atoms in the layer underneath. This structure is somewhat similar to Si(111)–(7 × 7). Ottaviano et al. [20] performed STS measurements on this surface and showed it has a band gap of approximately 0.8 eV. Eriksson et al. [30] revised the structural model by means of STM, STS, DFT (Density functional theory), ARUPS (Angle-resolved ultraviolet photo electron spectroscopy) and found that it consists of only 12 atoms in a unit cell (4 in the top layer and 8 in the layer below). His STM low voltage images (Fig. 3.6b) were able to resolve individual atoms in the under layer.

3.3 Indium on Si(111)

Indium is an element of III.A group and has one valence electron less than tin. This fact yields differences in the electronic structure of surfaces passivated by both elements. On the other hand, they are neighbours the in fifth period of the periodic table of elements and have a similar atomic radius, therefore we would expect some similarities in their behaviour on Si(111).

Lander and Morrison [32] first studied In reconstructions on Si(111) by LEED. They showed existence of eight 2D phases. Kraft et al. [33] performed STM and STS of all phases in the temperature range between 400–500 °C and constructed phase diagram (Fig. 3.8). Generally, structures transit from semiconducting to metallic with increasing coverage. In recent years, 4×1 reconstruction has gained a lot of attention due to its Peierls type [34] metal-insulator phase transition at

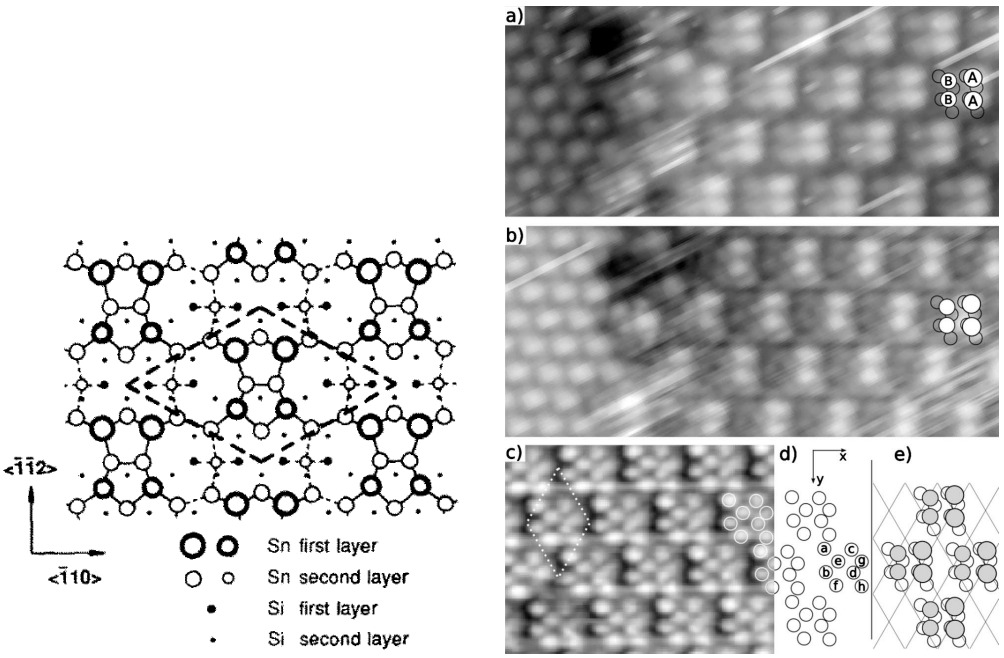

(a) (b)

Figure 3.6: (a) Topview of an atomic model for the Sn/Si(111)–($2\sqrt{3} \times 2\sqrt{3}$) R30° reconstruction proposed by [21] . The size of the unit cell is indicated with dashed rectangle. (b) Room temperature STM images of revised double layer model 3.6a. a) and b) show the same area at 0.5 and 0.1 sample bias respectively. Adjacent $\sqrt{3}$ reconstruction on the left. AA and BB pairs in the top layer are clearly visible in a) and AA and underlayer is visible in b). c) Image at 0.1 V bias of a different area where an eight-atom underlayer is clearly seen. d) Atomic positions of the underlayer. e) The underlayer and top layer (open and solid gray circles, respectively). The grid vertices correspond to the positions of the Sn atoms in the $2\sqrt{3}$ area (T_4 sites).

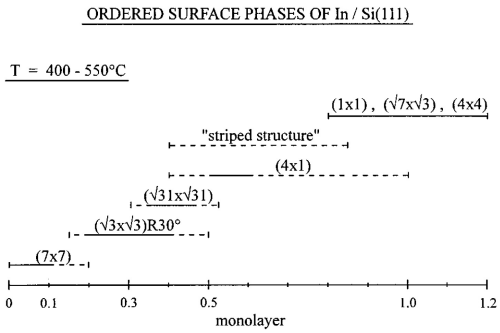

Figure 3.7: Phase diagram of In on Si(111) for temperatures of 400–500 °C based on images obtained by STM. [33]

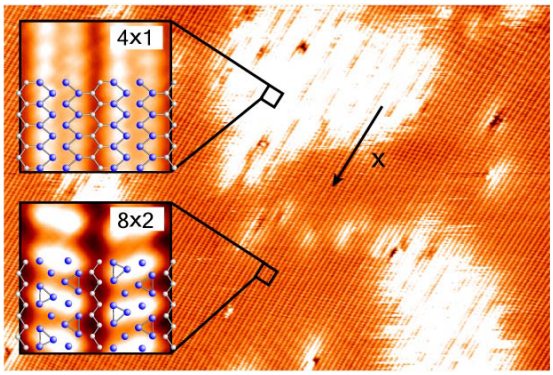

Figure 3.8: STM image depicting the In phase transition from room temperature 4×1 to low temperature 8×2. Image was taken at 121 K (corresponding to Curie temperature), with the sample bias of 0.7 V and the tunneling current of 100 pA. The insets are 5×5 nm^2 and the full image 150×100 nm^2.[35]

low temperature [35]. Metallic phase 4×1 changes into an insulating 8×2 at temperatures 100–130 K (see Fig. 3.8). The details of this effect are not well understood yet.
We are most concerned about the $\sqrt{3}$ reconstruction which also exists for indium (see Fig. 3.8) and about how does it compare to its Sn $\sqrt{3}$ counterpart.

3.3.1 In/Si(111)–($\sqrt{3}\times\sqrt{3}$) R30°

In STM, this reconstruction looks very similar to the Sn one with its coverage exactly 1/3 ML (if we exclude defects) [33]. There were discussions if In atoms are on top (T_4 position) or if the structure is relaxed and In atoms take the H_3 position but it is now generally agreed the former is the case [36]. Two types of defects are clearly recognized – substitutional Si defects and vacancies. Vacancies appear the same as on the Sn surface – dark in both empty and filled states. Furthermore, the vicinity of vacancy defect appears darker and it is most pronounced for filled states. Si-substitutional defects look comparable to their Sn counterparts in empty states at sample bias 2 V; they are dark but noticeably lighter than vacancies (see Fig.3.9). In filled states and sample bias between 1–2 V, they are shining much brighter than In atoms, indicating high LDOS [37]. At 2.5 V sample bias, their brightness in STM image is only slightly higher than the indium one.

We might prepare the $\sqrt{3}$ reconstruction either by deposition of larger amount approximately 1 ML of indium on clean Si(111) and then anneal it at 550 °C for sufficiently long period of time (Kraft et al. [33] did it this way) or deposit appropriate amount – slightly more than 0.3 ML – and anneal it for shorter period. In the first case, areas with the $\sqrt{31} \times \sqrt{31}$ might resist, especially close to surface steps, and their removal requires higher temperature which increases the amount of Si-substitutional defects. If we want to prepare the reconstruction with defined amount of substitutional defects and avoid the occurrence of the $\sqrt{31} \times \sqrt{31}$ islands, depositing appropriate amount of In atoms is the most controllable way how to do that.

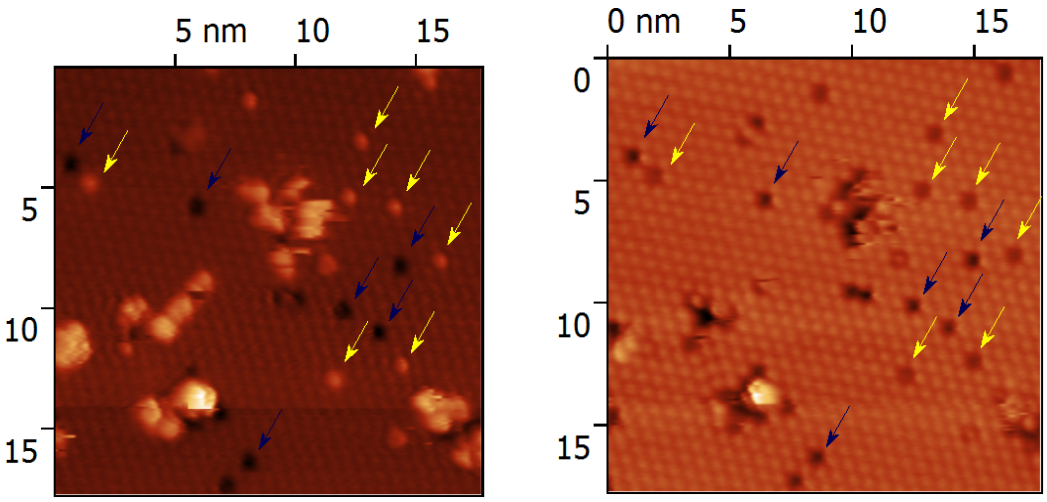

(a) (b)

Figure 3.9: (a) Filled and (b) empty state STM image of the $\sqrt{3}$ indium reconstruction with deposited 0.05 ML F_8CuPc molecules taken at sample bias $U_S = -2$ V (forward scan) respectively 2 V (backward scan) and tunneling current 0.3 nA. Vacancies are marked with blue arrows and Si-substitutional defects with yellow ones.

4. Molecules on surfaces

The research of molecules on surfaces was undoubtedly initiated by Aviram and Ratner [38] with their proposal of a current rectifier based on a single molecule. They are now considered as the gurus of molecular electronics though their work was only of a theoretical character. With the development of STM and non-contact atomic force microscopy in 1980s, an intensive experimental research of single molecules on atomic surfaces has begun. The general purpose of the new field called "molecular-scale electronics" is to construct electric circuits from single molecules or functional blocks build from molecules [39]. Electrical components such as rectifiers (diodes), transistors, switches and wires has to be made in a defect-free, reproducible and mass production in order to make molecular electronic available. Nowadays, molecular-scale electronics is still in its infancy and there is plenty of room for the research. Self-organization of molecules on surfaces is so called bottom-up approach that could enable building reproducibly large arrays of molecular devices and a big part of academic research on molecules on surfaces deals with it. Some researches also try to observe and synthesize molecular blocks on surfaces that will act as some of the previously mentioned electric components on the nanoscale.

4.1 Phthalocyanines

Phthalocyanines are a group of organic compounds consisting of 4 isoindole units that are linked together forming a macro-cyclic ring. They are widely used as dyes and, in recent years, they have begun to be used as organic semiconductors in e. g. organic solar cells [40]. There is a large group of metallophthalocyanines (MPcs) that have a metal atom in their centre (see Fig. 4.1a). Although the structure of all MPcs is similar and two electrons mediate the bond of phthalocyanine cycle with the central atom in all cases, their physical and chemical properties are different. There is a special case of phthalocyanine without the central metallic atom – called simply phthalocyanine or metal-free phthalocyanine (H_2Pc) with two hydrogen atoms bonded in the centre (see Fig. 4.1b). At room temperature for similar porphyrine molecule, there is a permanent tautomerization of inner hydrogens – changing the conformation from 1–3 to 2–4 positions with rate 1.7×10^4 Hz [41], however, in an adsorbed state the tautomerization can freeze even at room temperature [42]. The tautomerization rate of H_2Pc in crystal at room temperature was estimated to 10^5 Hz (activation energy is 0.4 eV) by NMR (Nuclear magnetic resonance spectroscopy) [43], however for isolated molecule the rate is in order of Hz and the activation energy was calculated using DFT as 0.66 eV (considering the pre-exponential factor as $\approx 10^{11}$ from [43] it yields the rate 0.7 Hz using Arrhenius equation) [44]. This was also confirmed experimentally at glass/air interface under ambient conditions ans at room temperature where the rate was measures as $0.25 - 2$ Hz [45]. Phthalocyanines have many interesting properties [46] which make them commonly used in surface science and electronics with potential application in single molecule electronics. Some of them are:

1. ease of crystallization and sublimation

2. high thermal stability (decomposition temperature 500°C in air and 900°C in vacuum)

3. large extended π conjugated system containing 18 electrons and resulting in HOMO-LUMO[1] gap in visible light spectrum and an intensive absorption

4. versatile chemical system with electronic properties tunable by substitution of the central metal atom (more than 70 elements possible) or the outer hydrogen atoms e. g. by fluorines (Fig. 4.1d) and a change from p-type semiconductor (CuPc) to n-type semiconductor (F_{16}CuPc)

In our research group, until now, four types of phthalocyanines (see Fig. 6.10) deposited on passivated silicon surfaces have been studied. The first, copper phthalocyanine (CuPc) is the most common type of phthalocyanine. Its relatives copper octafluorophthalocyanine (F_8CuPc) and copper hexadecafluorophthalocyanine (F_{16}CuPc) were chosen to observe how electronegative fluorines affect adsorption behaviour. In case of H_2Pc, absence of the central atom can play an important role in adsorption. Moreover, for performing a DFT study, H_2Pc is an easier system to calculate than the CuPc one.

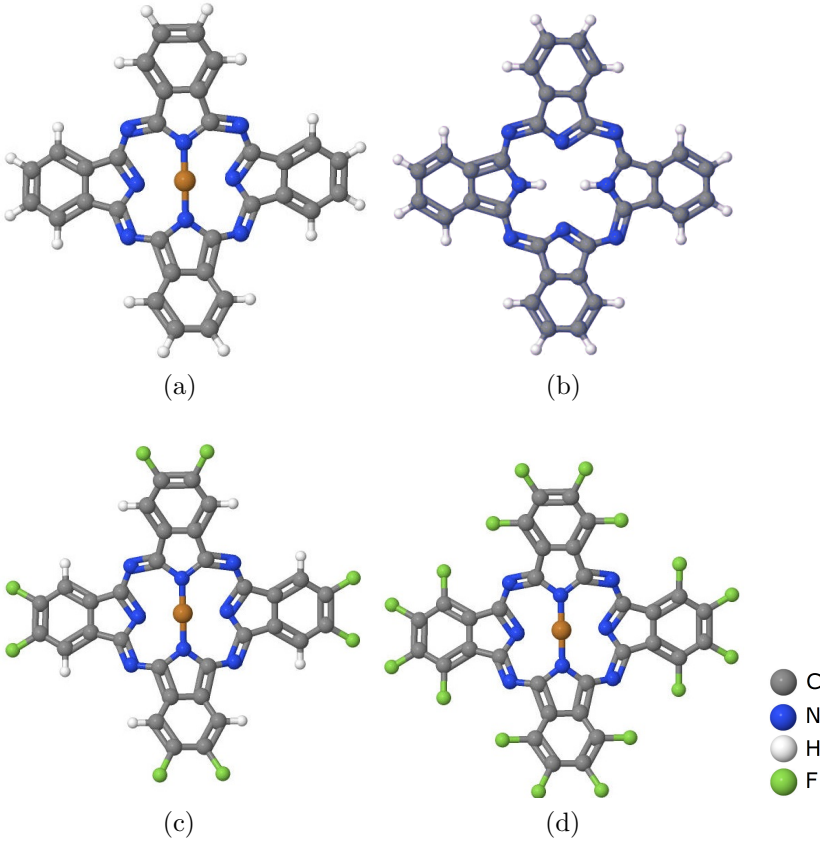

Figure 4.1: Structural model of phthalocyanine molecules. a) CuPc b) H_2Pc c) F_8CuPc d) F_{16}CuPc

[1]HOMO means highest occupied molecular orbital and LUMO means lowest unoccupied molecular orbital

[htbp]

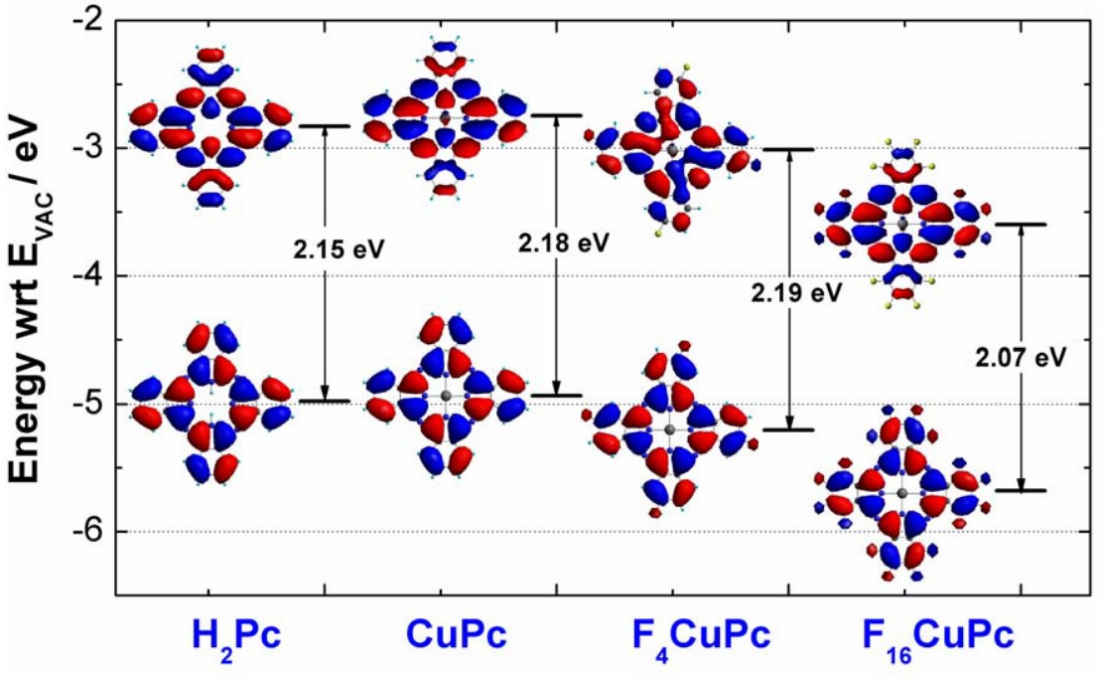

Figure 4.2: The DFT estimated transport gaps of H_2Pc, CuPc, F_4CuPc and $F_{16}CuPc$ on Si(111)-H and their HOMO and LUMO charge distributions. [47]

4.1.1 DFT calculations of molecular orbitals

The ball structural model is not sufficient if we want to know how are phthalocyanines imaged by STM. DFT calculations of molecular orbitals (charge density clouds) give us a better idea how phtalocyanines look like in STM. There are several calculations in the literature of the HOMO and the LUMO of phthalocyanines. One of them is depicted in Fig. 4.2. Positive charge is denoted with red colour and negative charge with blue or green colour. Even though author of the PhD thesis [47] claims that the DFT is calculated for molecules on the Si(111)-H, the HOMO and the LUMO model was most probably calculated for a free-standing molecule. The calculated model for H_2Pc is in general agreement with models of others [48]. The CuPc molecule is more difficult to calculate, hence I also attach calculations from other source [49], already peer-reviewed. In our measurements, we use F_8CuPc molecules with fluorines in (β_1, β_2) positions (see Fig. 4.2 and 4.4). From Fig. 4.4 it is evident that the HOMO and the LUMO in the centre of all used F_xCuPc molecules look the same, only on positions where fluorines are substituted, charge excess is visible due to the higher electronegativity and larger atomic radius of fluorine in comparison with hydrogen.

4.2 Phthalocyanines on surfaces

Phthalocyanines (and generally all molecules) began to be first studied by means of STM in late 1980s on metal surfaces (most commonly Ag, Cu and Au). They usually adsorb in a flat-lying configuration parallel with the surface due to a Van der Waals interaction. At coverages close to 1 ML they often form an ordered structure. This is mostly a result of the Van der Waals interaction and also de-

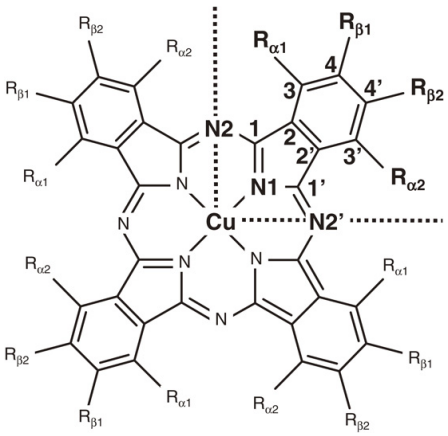

Figure 4.3: Molecular structure of F_xCuPc used for calculation. $R_{\alpha 1}$, $R_{\alpha 2}$, $R_{\beta 1}$ and $R_{\beta 2}$ represent hydrogen or fluorine atoms. [49]

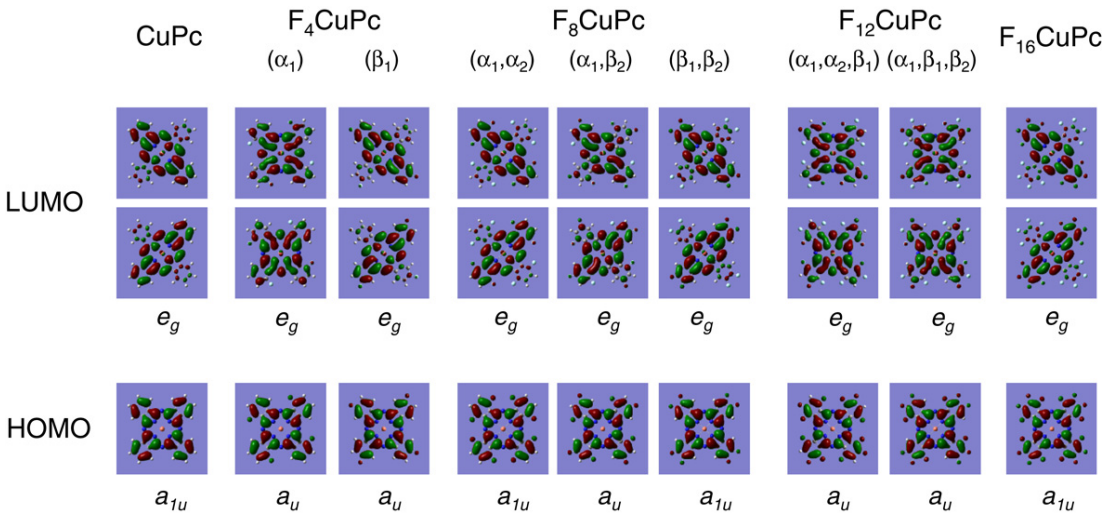

Figure 4.4: Wave functions (charge density) of HOMO and LUMO calculated for F_xCuPc. The LUMO levels are double degenerated in all cases. [49]

pends on the potential energy landscape of the surface. At room temperature on weakly interacting metal surfaces (Au, Ag) and also on passivated semiconducting surfaces they can be mobile and unable to be directly seen in STM. Matvija et al. [50] provided a different approach to the problem and visualized 2D molecular gas on surface by means of STM and characterized it with a pair correlation function. Decreasing the temperature down to few Kelvins, molecules do not have enough thermal energy to overcome diffusion barriers, are frozen – fixed to certain position – and single molecule effects can be studied.

Semiconducting surfaces have unsaturated dangling bonds which provide capture sites for phthalocyanines deposited on surface. π conjugated molecular orbital interact with e. g. a Si dangling bond and forms a covalent bond [51] (chemisorption) with binding energy orders of magnitude higher than the Van der Waals interaction. Breaking the bond is not in most cases possible without heating the surface up to very high temperatures which would first cause dissociation of molecules. Although covalent bond is beneficial for charge transport, the impossibility of selective adsorption and self-organizing of most of the molecules on Si(100) and Si(111) surfaces hinders its application in molecular electronics.

On silicon surfaces passivated by hydrogen the situation is different. More adsorption positions are present, molecules (CuPc) can sit on a dangling bond of Si(100)-H either with the metal atom or with a benzene ring in one of the four lobes resulting in a rotation of the molecule around the axis of the bond perpendicular to the surface and a circle-like appearance in the STM [52]. On Si(111)-H random adsorption is present at coverages less than 1 ML. The strong covalent bonding of phthalocyanines on bare silicon surfaces usually drastically disrupts electron structure of the molecule and the typical 4-fold or 2-fold rotational symmetry in an STM image is not present. On the contrary, on passivated surfaces, molecules often maintain their symmetrical shape. Until now, adsorption of molecules on passivated Si(111) was most studied on silver and boron terminated surfaces, both exhibiting the $\sqrt{3} \times \sqrt{3}$ reconstruction. For the latter surface, there already exists a review paper [53]. Wagner et al. studied adsorption of 3 types of phthalocyanines (ZnPc, CoPc and CuPc) at liquid nitrogen temperature and clarified differences between each other with the help of a DFT calculation. The central transition-metal atom plays a crucial role in the interaction with the substrate due to the different valence resulting in a different p-d orbital coupling (p is from the silicon adatom and d is from the transition-metal atom).

There are not many papers on adsorption of molecules, specifically phthalocyanines, on silicon surfaces passivated by indium and tin — only a few in the last 5 years, most often from people who were studying these surfaces without molecules before (see chapter 3). PTCDA molecule (Perylenetetracarboxylic dianhydride) tends to self-organize at room temperature (RT) on In/Si(111)–(4×1) [54], Sn/Si(111)–$(2\sqrt{3} \times 2\sqrt{3})$ R30° [55, 56] but not on e. g. In/Si(111)–$(\sqrt{31} \times \sqrt{31})$ [54] or on Sn/Si(111)–$(\sqrt{3} \times \sqrt{3})$ R30° where the molecule chemically reacts with the surface [57] which results in breaking the molecule and disordered growth [56]. C_{60} fullerene molecules behave different from phthalocyanines and other π conjugated molecules, but they were studied on In/Si(111)–$(\sqrt{3} \times \sqrt{3})$ R30° by Gruznev et al. [58] and two interesting effects were observed. Firstly, it was found that at low C_{60} coverage (0.01 ML) on a surface with approximately

4 % of Si-substitutional defects 75 % of all adsorbed molecules are tied to these defects, approximately 20 % are tied to other C_{60} and only 5 % are bound individually on the surface at RT. It was shown that the C_{60} with a mean diameter around 0.7 nm [59] (comparable with $\sqrt{3}$ lattice constant 0.66 nm) occupies most probably on-top positions of In atoms neighbouring the Si defect. Secondly, it was found that a group of C_{60} can act as a trap for "mobile vacancies". There are generally two types of vacancies at RT: "mobile" and "immobile". The latter have extrinsic origin in the impurity atom in the subsurface region close to the vacancy. Due to the negligible bulk diffusivity of this impurity at RT, the vacancy is "immobile". The "mobile" vacancies are believed to be intrinsic surface defects and could change their position simply by In atom hopping. The origin of the "mobile" vacancy trapping is in a strain induced in the indium layer by C_{60} and a position shift of the In atoms in between the fullerenes and the vacancy from the T_4 to the H_3 sites which results in vacancy anchoring. From Gruznev et al. study one has to take into account that not only the defects themselves could act as traps for molecular adsorption, but also the perturbed neighbourhood of the substitutional defect plays an important role.

4.3 Molecular switches

Molecular switch is a device made from a molecule which can be reversibly switched between two or more stable states. The switching could be done by external stimuli like light, temperature, electric field, change in the external environment, etc. The problem of these stimuli is a lack of the single molecule selectivity. The STM tip is a unique probe which can induce molecule switching or more generally manipulate the molecule and its states. This could be done in several ways according to the physical effects involved:

- Very high electric field in the vicinity of the tip apex. When applying bias voltage between the tip and the sample, an electric field is created causing a force that acts on molecule with the dipole moment.
- Tunneling current. Inelastic tunneling of electrons or holes can excite molecular vibrations and transport certain portion of energy to the molecule – locally heat it.
- Quantum-mechanical interaction. Approaching the tip very close to the molecule causes overlapping of the tip and the molecular orbitals which results in a change in the electronic structure and the force interaction between the last atom on the tip and the nearest atom in the molecule.

There is an evidence of phthalocyanine molecules that exhibit switching when probed by STM. In several non-planar metallophthalocyanines – SnPc [60, 61], VOPc [62] or ClAlPc [63] pulling or pushing the central metal atom or functional group through the molecular plane is possible with the STM tip. This is done either by a voltage pulse or a Z-ramp (controllable approach of the tip towards the surface and back). In the case of SnPc on Ag(111) the switching is not reversible unless the switched molecule sits in the second molecular layer and is decoupled from the surface. Another, probably the most famous example of switching is

tautomerization of hydrogen atoms in metal-free naphthalocyanine and phthalocyanine on ultra-thin insulating NaCl, RbI and Xe films on a copper monocrystal. All described switchings stem from effects related to inelastic tunneling, although, all the experiments were performed at temperatures of few Kelvins. Kumagai et al. [64] intensively studied porphycene molecule on Cu(110) by STM. Porphycene is a π conjugated molecule dimensionally comparable to phthalocyanine with a rectangular rather than square geometry like phthalocyanine or porphyne. Two hydrogen atoms are in the inner cavity and can exhibit cis-cis tautomerization. At 5 K this tautomerization occurs at certain threshold voltage where inelastic tunneling channel opens and its switching rate is dependent on the voltage and exhibits I^N dependence on the tunneling current where N is a number of electrons involved in a single electron process. However, at higher temperatures between 70–90 K, there is no observable dependence of the switching rate on tunneling current and the process is thermally activated and follows Arrhenius equation.

4.4 Fuzzy imaged phthalocyanine molecules on passivated silicon surfaces

In our Thin Films group, adsorption of phthalocyanines on passivated silicon surfaces is the subject of ongoing research. Until now, CuPc, F_{16}CuPc and H_2Pc molecules were studied on Sn/Si(111)–($\sqrt{3} \times \sqrt{3}$) and H_2Pc moreover on In/Si(111)–($\sqrt{3} \times \sqrt{3}$). It was found that molecules adsorb only on defects and fuzzy imaged CuPc and H_2Pc were observed on Sn/Si(111)–($\sqrt{3} \times \sqrt{3}$). By a controlled approach of the tip of approximately 0.8 nm, the "fuzzy" molecule was removed and a Si-substitutional double defect appeared on the original location of the molecule (see Fig. 4.5). The same molecule was also observed "fuzzy" on the In/Si(111)–($\sqrt{3}\times\sqrt{3}$) either on the Si double defect or on the Si triple-defect (the angle between the lines that connect the two neighbouring Si atoms is 120°). The "fuzzy" molecule on the In/Si(111)–($\sqrt{3}\times\sqrt{3}$) seemed to be bound weaker to the defect and sometimes, spontaneous desorption occurs and the Si substitutional double or triple defect is found on the original location of the molecule.

At certain scanning conditions (see Fig. 4.6) a CuPc molecule remained a moment in one absorbed state, then in the other – mirror-symmetrical to the previous state along the connecting line of the double defect – and finally remained in a fuzzy state.

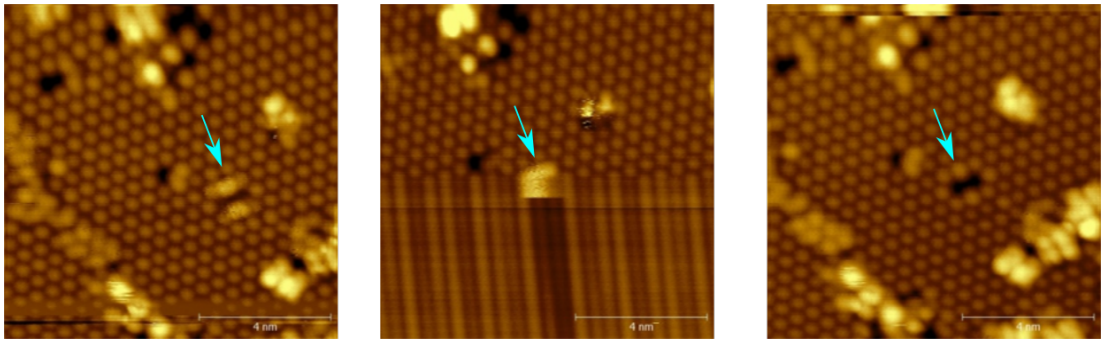

Figure 4.5: Removal of fuzzy imaged CuPc (marked with blue arrow) from Si-substitutional double defect on the Sn/Si(111)–($\sqrt{3} \times \sqrt{3}$) by controlled approach of the tip during scanning single line over the molecule with disabled feedback loop – in constant height mode. Taken with permission from [65].

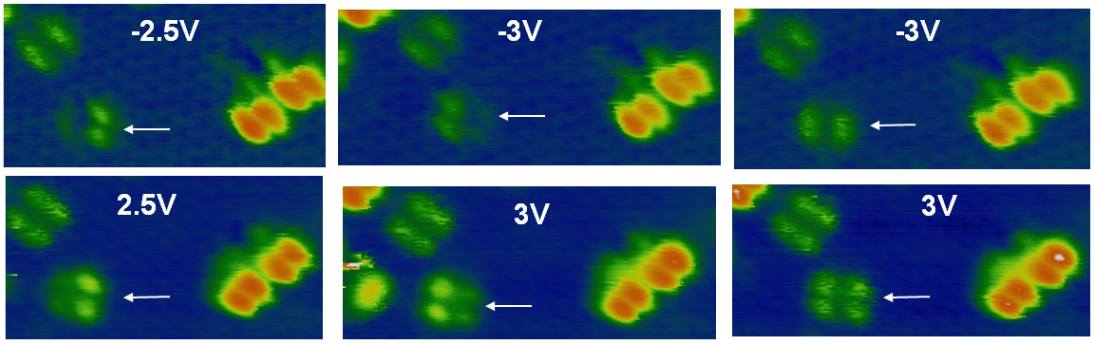

Figure 4.6: A hop of a CuPc molecule (marked with white arrow) from one adsorbed state to the other (type X overturn) and finally to fuzzy imaged state where it remained. Tip voltage is marked in each image and the surface is the Sn/Si(111)–($\sqrt{3} \times \sqrt{3}$). Taken with permission from [65].

5. Experimental STM apparatus

Our UHV STM apparatus is home-built. The STM head was constructed by doc. Ivan Ošťádal and the electronics and control software was designed and implemented by doc. Pavel Sobotík.

5.1 Construction of the apparatus

The photo of the apparatus is in Fig. 5.1. The body of the apparatus is crafted from stainless steel and each flange is sealed with a copper or a wheaton gasket. Only one main vacuum chamber is present in which the STM head and evaporators are located. During the experiments, base pressure is kept in the order of 10^{-9} Pa. This is achieved by a multi-level pump system. It consists of an ion pump, a two-level turbomolecular pump prevacuumed by a membrane vacuum pump and a titanium sublimation pump. The ion pump is the only pump that can operate during scanning since it does not cause any vibrations. The titanium sublimation pump is used before each experiment and the remaining two pumps are used only after aeration of the chamber when the UHV conditions have to be achieved again. The complete vacuum scheme can be found in [66]. Pressure is measured by a hot-filament ionization gauge.

Silicon samples are n-types Sb-doped with resistivity $< 1 \times 10^{-2}$ Ωm. They are located in the holders attached on a rotary carousel as depicted in Fig. 5.2. The Platinum crystal and the tungsten metal plate are also on the carousel. The sample on the site adjacent to the tip is contacted when the STM head hangs freely and the sample on the opposite site (facing the evaporators) is contacted when the STM head is locked. With this clever mechanism the preparation of the samples and scanning is very user-friendly, because one has to change the position of the desired sample by rotating the carousel only between the two positions described above.

There are two locations of evaporators, as can be seen in Fig. 5.2. A tin and an indium evaporator is formed from a tantalum crucible and it is wrapped by a tungsten wire that is resistively heated. Phthalocyanine evaporators are made from a boron nitride crucible and are heated in the same way.

Samples are prepared by resistive heating and there is not a possibility to measure their temperature. We can therefore tune only the power consumption of them. The calibration of temperature dependence on input power was done for different silicon samples using thermocouple attached to them and is portrayed in Fig. 5.3. It is evident that the dependence of temperature on the power is linear with different coefficients for different samples. From the graph, we can estimate the temperature based on the power with an accuracy of approximately 15 %. Samples can be also heated in the position under the tip during scanning. This enables to operate our STM from room temperature up to several tens of degrees of Celsius.

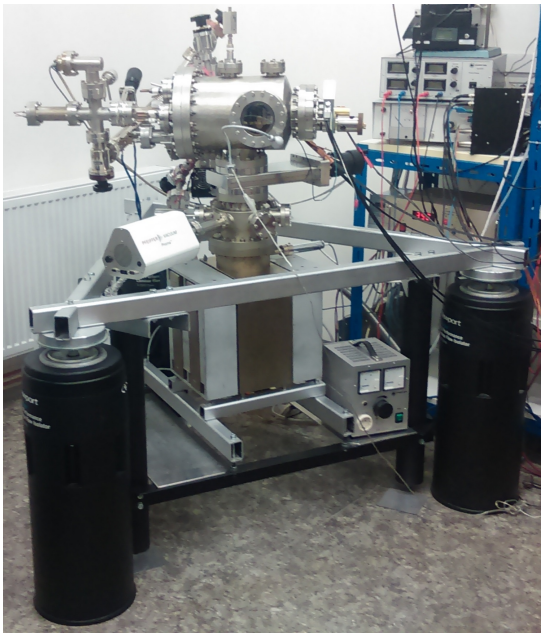

Figure 5.1: The photo of the STM apparatus located in the Thin Films group laboratory.

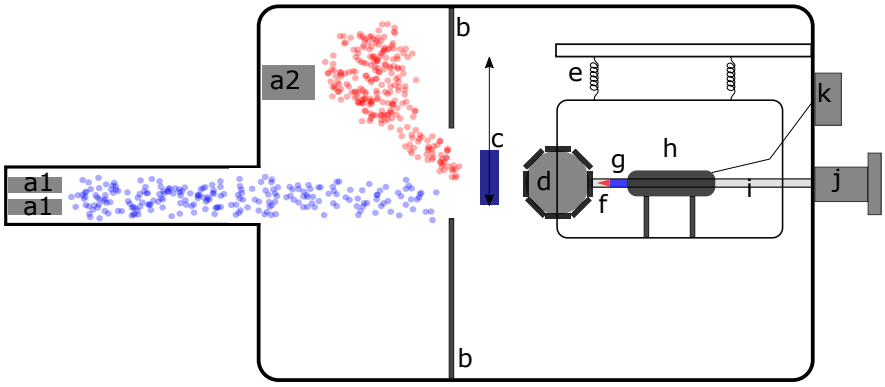

Figure 5.2: Schematic drawing of the vacuum chamber of our STM apparatus. a1) phthalocyanine evaporators, a2) Sn, In an Tl evaporators – molecular beam is depicted with coloured circles , b) shading plate, c) quartz-microbalance thickness monitor with the illustrated path of its range of motion, d) rotary carousel with 8 sample positions, e) internal cage hung on coils and damped by an eddy current system, f) tungsten tip, g) piezoceramics, h) Inchworm linear motor, i) axis of the rotary manipulator which turns the carousel, j) rotary motion feedthrough, k) electric feedthrough and electrical amplifier.

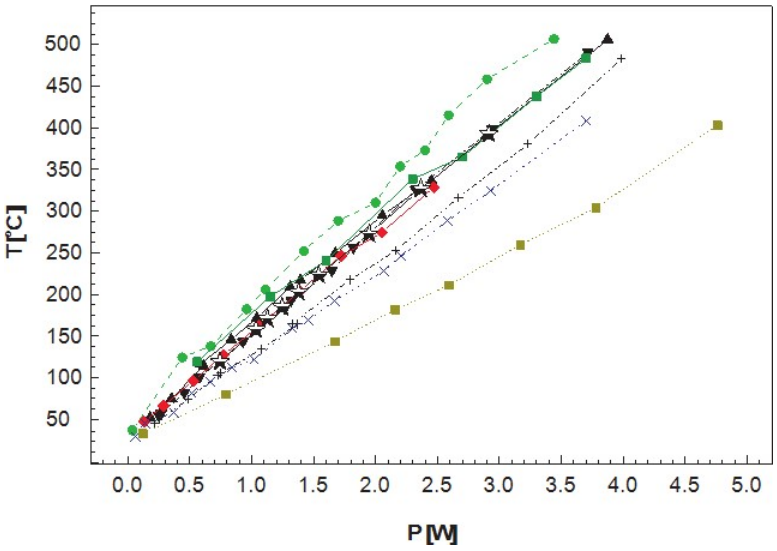

Figure 5.3: Temperature calibration of different Si samples [67]

6. Results

All experiments were carried out using room temperature UHV STM apparatus. A silicon Si(111) sample was cleaned by repeated flash-annealing to 1200 °C for 15 s. The sample was resistively heated by direct current and after each annealing step the polarity of the source was changed. During the repeated annealing procedure the pressure stayed below 3×10^{-8} Pa and during the last step of the annealing, the pressure stayed below 1×10^{-8} Pa. The preparation of high quality 7×7 reconstruction requires slow cooling (1°C/s) between 900-700 °C after the last step of annealing. However, for the subsequent Sn/In deposition and the preparation of the $\sqrt{3}\times\sqrt{3}$ reconstruction it was not needed to have the 7×7 reconstruction beforehand and the sample was quenched immediately. The deposition rate of the tin and the indium evaporators was in the range of $1 - 1.5 \times 10^{-3}$ ML/s (1 ML corresponds to one atom of adsorbate to one atom of Si(111) surface, 1 ML $= 7.83 \times 10^{14}$ atoms $\cdot$ cm^{-2}) and the rate of the phthalocyanine evaporators was between $0.5 - 1 \times 10^{-3}$ ML/s (1 ML corresponds to one molecule to 15 atoms of Si(111) surface – closed packed structure, 1 ML $= 5.22 \times 10^{13}$ molecules $\cdot$ cm^{-2}). The deposition rate was measured by a quartz micro-balance monitor that was placed on the shutter between the evaporator and the sample. Hence, it was necessary to wait until the flux of particles became constant in time and then the shutter was opened and the rate was considered as the rate before the opening. The calibration of the exact deposition rate was done by previous users of the STM and the error can be estimated as 10 % [66].

6.1 Image processing

STM image was acquired during forward (FW) and backward (BW) scanning. In each direction, the topography (tip position) and the tunneling current were measured and FW and BW current and topography images were generated and packed all together in *.img* format. This format was transformed to Gwyddion [68] software which was used for the whole processing. In constant current mode only the topography image was further processed. The processing simply consisted of levelling the data through plane subtraction and the alignment of the rows using median or median of differences methods. In the case of the "fuzzy" imaged molecules, neither horizontal scars removal nor filtration were used, since it might drastically change the appearance of the object present. Current images acquired in constant height mode were processed identically, but a logarithm of the current (vertical colour scale) was calculated in order to rescale the tunneling current to distance.

6.2 I(V) and I(t) processing

STS spectra were measured using lock-in technique. In all cases lock-in amplifier was used to acquire $\mathrm{d}I/\mathrm{d}V$ curve with a modulation frequency of 965 Hz and an amplitude of the modulation voltage 50 mV. Simultaneously, I-V curve was measured and used for normalization. Each spectrum contains 2000 points and the acquisition time for one point was 50 ms. Similar spectra from equivalent positions were summed up and smoothed. Smoothing was done using Savitzky-Golay filter in Scipy Python software with a window length of 101 points for $\mathrm{d}I/\mathrm{d}V$ curve and 301 points for I-V curve. In order to avoid the divergence of $(\mathrm{d}I/\mathrm{d}V)/(I/V)$ we used the relation described in [69]

$$\text{normalized } \mathrm{d}I/\mathrm{d}V \sim (\mathrm{d}I/\mathrm{d}V)/\sqrt{(I/V)^2 + c} \tag{6.1}$$

where c is a small constant ($c = 0.005$ was used for all spectra). The normalized $\mathrm{d}I/\mathrm{d}V$ obtained was finally filtered with Savitzky-Golay with a window length of 51 points.

Time series of the tunneling current was acquired over H_2Pc and F_8CuPc fuzzy imaged molecules. In our measurements the maximum possible number of acquired points of the series is 16384 and it was used in all cases. In the case of the series for H_2Pc, sampling frequency 20 kHz (0.05 ms per point) was used which determined the length of the series as 819 ms. For the F_8CuPc molecules, time series was acquired at sampling frequency $16.\overline{6}$ kHz (0.06 ms per point) due to the change of the internal frequency of the STM control software. Resulting recorded time was 983 ms. One has to keep in mind that the bandwidth of the pre-amplifier is different for various gains (V/A). For H_2Pc a gain of 10^8 was used and its upper cut-off frequency was 7 kHz. For F_8CuPc a gain of 10^9 was used with considerably smaller upper cut-off frequency 1.1 kHz.

For the two state fluctuations apparent in the time series, filtering was necessary since the two current levels were sometimes mixed together. We applied median filtering to all of the series with both left and right ranks of 5 points (0.25 ms and 0.3 ms respectively). The effect of filtering on the calculated parameters was examined on a time series with low noise level and we can say that the filtering increase the mean lifetime to a maximum of 15% compared to reality. After filtering the data, threshold current was manually determined from the current values histogram and the values below the threshold were considered as the state 1 (low) and the values above the threshold as the state 2 (high).

6.3 List of performed experiments

Prior to each measurement of molecules on surfaces, the quality of clean surface was checked in STM. The tip was reshaped by procedures described in the first chapter and the atomic resolution and a metallic I-V character were obtained since regaining the resolution on surfaces with molecules is difficult. Both tin and indium passivated surfaces were prepared by annealing after metal deposition of 0.4 ML to create the $\sqrt{3} \times \sqrt{3}$ reconstruction with appropriate amount of Si-substitutional double defects. The constant input heating power was maintained by a PID controller. The temperature that corresponds to the annealing power of

3 W is $T = (350 \pm 50)$ °C and can be estimated from Fig. 5.3. All measurements were performed at room temperature $T_R = (25 \pm 3)$ °C.

The Sn/Si(111)–($\sqrt{3}\times\sqrt{3}$) R30° and the In/Si(111)–($\sqrt{3}\times\sqrt{3}$) R30° reconstructions were chosen in order to examine fuzzy imaged phthalocyanine molecules adsorbed on Si-substitutional double defects. The fuzzy behaviour indicates switching between two states which is also prominent in time series analysis as switching between two separate current levels. This is of great importance since switching of a molecule between two levels can be used in the molecular scale electronics. However, for successful application the switching should not be spontaneous and the changes of the state must be reversible. The H_2Pc and the F_8CuPc molecules were used since only these were available in evaporators in our chamber. It was also checked if there is any self-organization at 1 ML molecular coverage of F_8CuPc on the Sn/Si(111)–($\sqrt{3}\times\sqrt{3}$). No self-organization was observed and therefore no further attention was paid to surfaces with monolayer coverage.

meas. n.	surface	preparation (t, P)	molecules	Θ_m [ML]
1	In $\sqrt{3}$, $\sqrt{31}$	5 min, 3 W	x	x
2	In $\sqrt{3}$	5 min, 2.8 W	F_8CuPc	0.05
3	Sn $\sqrt{3}$	3 min, 2.7 W	H_2Pc	0.04
4	Sn $\sqrt{3}$	3 min, 2.7 W	H_2Pc	0.04
5	Sn $\sqrt{3}$	3 min, 2.7 W	H_2Pc	0.05
6	Sn $\sqrt{3}$	3 min, 2.7 W	H_2Pc	0.04
7	In $\sqrt{3}$	3 min, 3 W	H_2Pc	0.04
8	Sn $\sqrt{3}$	3 min, 2.9 W	F_8CuPc	0.04
9	Sn $\sqrt{3}$	3 min, 2.9 W	F_8CuPc	1
10	Sn $\sqrt{3}$	3 min, 2.9 W	H_2Pc	0.04

Table 6.1: Table of performed measurements. After deposition of 0.4 ML of metal, surface was annealed using PID regulation for time t with power P. $\sqrt{3}$ denotes the $\sqrt{3} \times \sqrt{3}$ reconstruction and $\sqrt{31}$ denotes the $\sqrt{31} \times \sqrt{31}$ reconstruction.

6.4 F_8CuPc on Sn/Si(111)–($\sqrt{3}\times\sqrt{3}$)

F_8CuPc molecules adsorb on the Sn/Si(111)–($\sqrt{3}\times\sqrt{3}$) R30° predominantly on Si-substitutional double defects at low coverage (see Fig.6.2) and they appear fuzzy in STM image on these defects with typical 2-fold rotational symmetry and no fuzzy behaviour above the axis connecting the double defect atoms (hereafter a_{dd}). At 1 ML coverage, molecules form disordered clusters which are being swept with the tip during scanning. Fuzzy molecules can be still seen adsorbed on the uncovered parts of the surface on Si-substitutional double defects. This indicates that once the defect is saturated by the molecule, presence of additional molecules in its vicinity does not cause reordering.

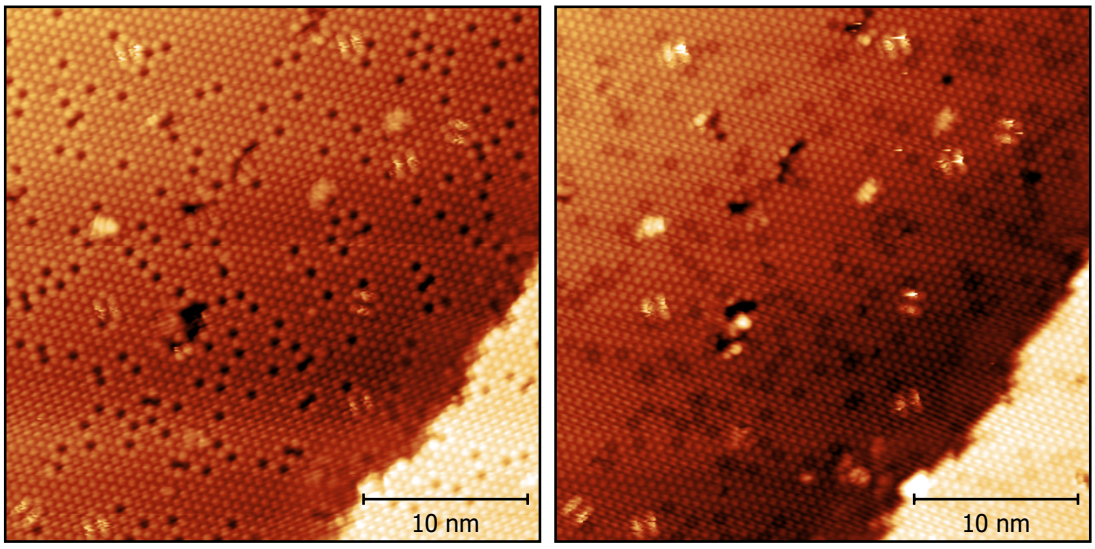

(a) Forward scan, U_S=-2 V (b) Backward scan, U_S=2 V

Figure 6.1: STM images of the Sn/Si(111)–($\sqrt{3}\times\sqrt{3}$)R30° with 0.04 ML of phthalocyanine molecules. (a) filled and (b) empty state image, tunneling current I_T=0.2 nA.

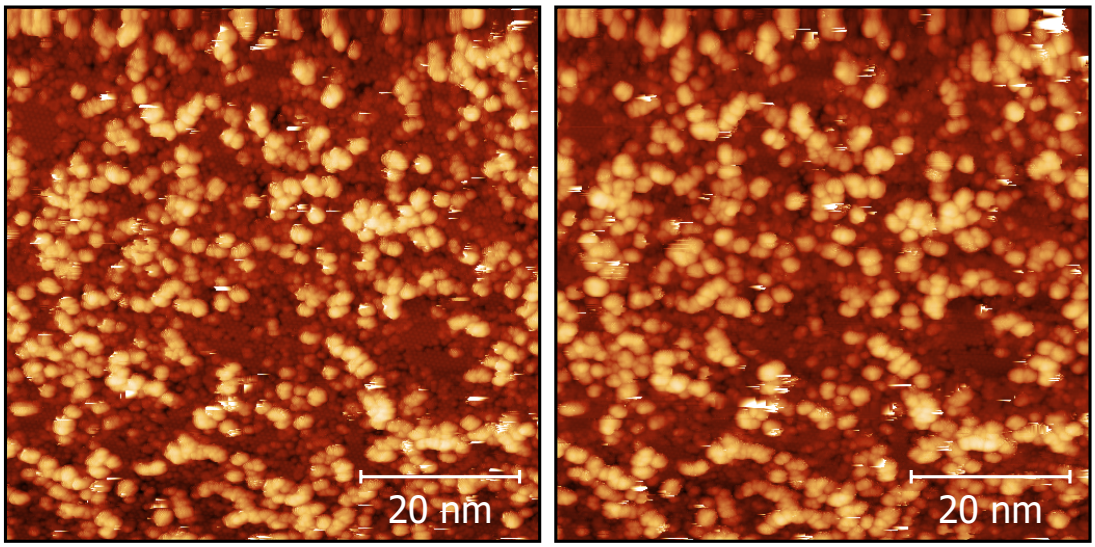

(a) Forward scan, U_S=-2 V (b) Backward scan, U_S=2 V

Figure 6.2: STM images of the Sn/Si(111)–($\sqrt{3}\times\sqrt{3}$)R30° with 1 ML of F_8CuPc phthalocyanine molecules. (a) filled and (b) empty state image, tunneling current I_T=0.2 nA.

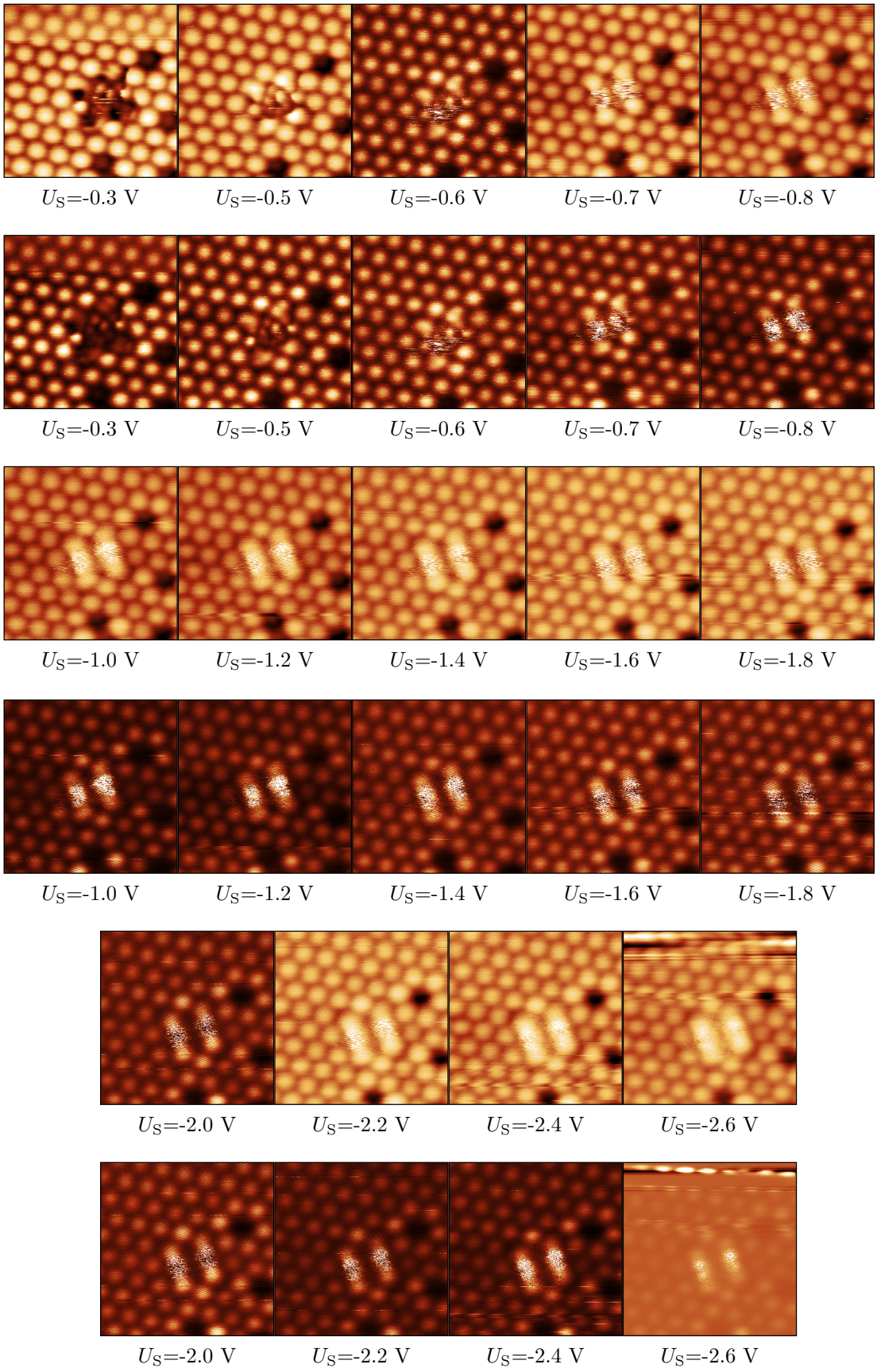

Figure 6.3: Voltage dependent STM images of fuzzy imaged F_8CuPc in filled states. First, third and fifth row – constant current mode I_T=0.05 nA in a forward scan, second, fourth and sixth row – corresponding images at the same sample bias taken in constant height mode in a backward scan. Scanning speed: 26 nm/s. Image size: 5×5 nm^2.

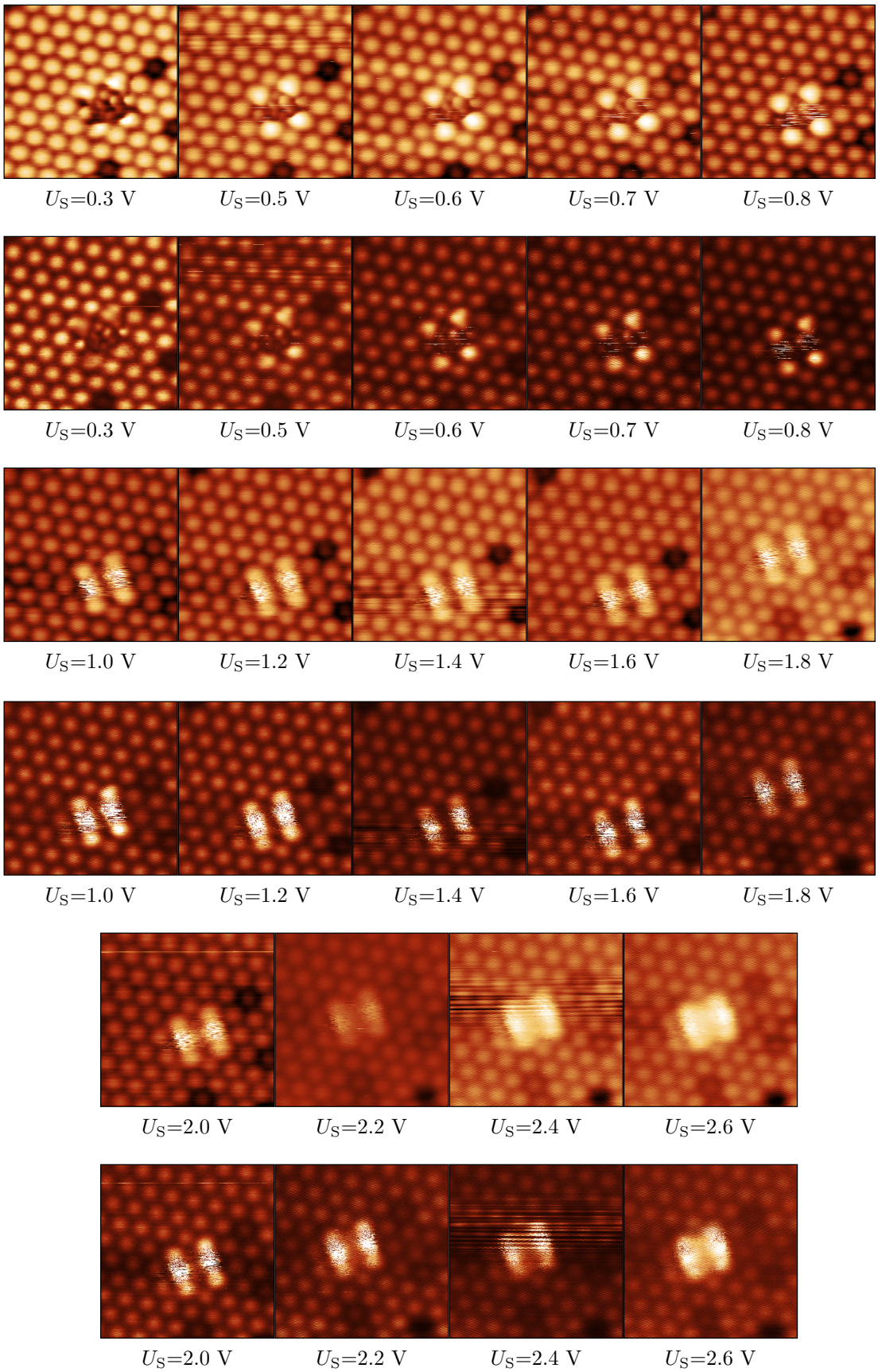

Figure 6.4: Voltage dependent STM images of fuzzy imaged F_8CuPc in empty states. First, third and fifth row – constant current mode I_T=0.05 nA in a forward scan, second, fourth and sixth row – corresponding images at the same sample bias taken in constant hight mode in a backward scan. Scanning speed: 26 nm/s. Image size: 5×5 nm^2.

6.5 H_2Pc on Sn/Si(111)–($\sqrt{3}\times\sqrt{3}$)

H_2Pc molecules at low coverage adsorb not only on Si-substitutional double defects (fuzzy appearance) but also on Si single defects and multiple defects (see Fig. 6.5). It is hard to distinguish between different configurations of adsorbed molecules because their resolution in STM is not very good. One of them (marked with blue arrow), very bright in both empty and filled states with no symmetry and resolved lobes, can be seen. Others are most prominent in empty states e. g. double-bean shape imaged molecule (yellow arrow). Three-lobe imaging was also sometimes present and spectra were measured on it (Fig. 6.14a). Fuzzy imaged molecule on double defect (green arrow) can be always clearly recognized when the tip is sufficiently good to resolve Sn/Si(111)–($\sqrt{3}\times\sqrt{3}$) surface features.

Influence of scanning direction on the imaging of the "fuzzy" molecule is shown in Fig. 6.9. We can see that the shape of the fuzzy area is the same for scanning in the direction of axis a_{dd} and scanning in the perpendicular direction. The pushing or pulling of the molecule by the tip in the direction of scanning can be therefore excluded.

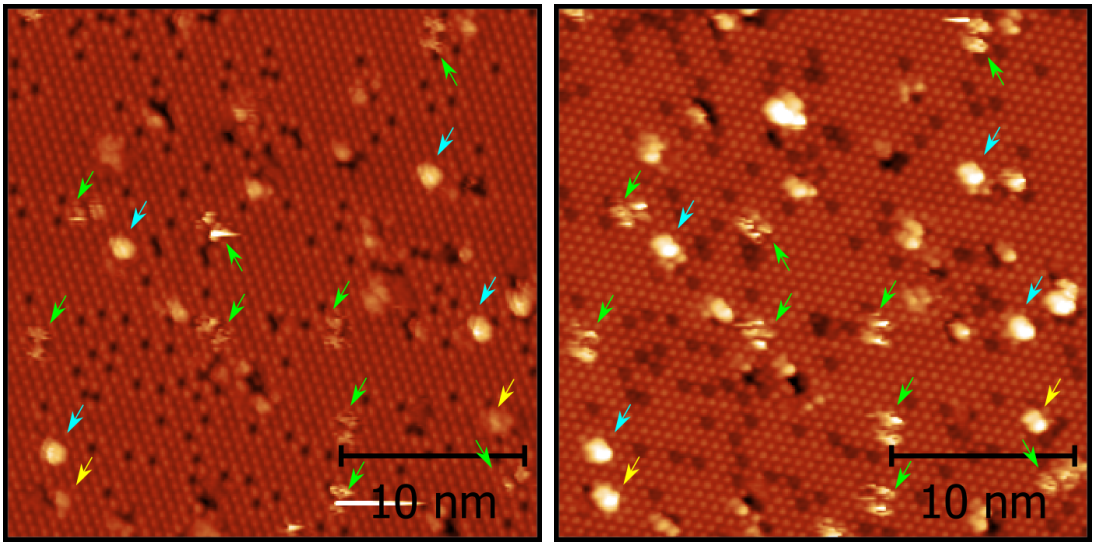

(a) Forward scan, U_S=-2 V (b) Backward scan, U_S=2 V

Figure 6.5: STM images of the Sn/Si(111)–($\sqrt{3}\times\sqrt{3}$)R30° with 0.05 ML of H_2Pc phthalocyanine molecules. (a) filled and (b) empty state image, tunneling current I_T=0.3 nA. Different imaging of molecules marked with arrows. Green arrow: fuzzy imaged molecule, blue arrow: bright molecule, yellow arrow: double-bean molecule

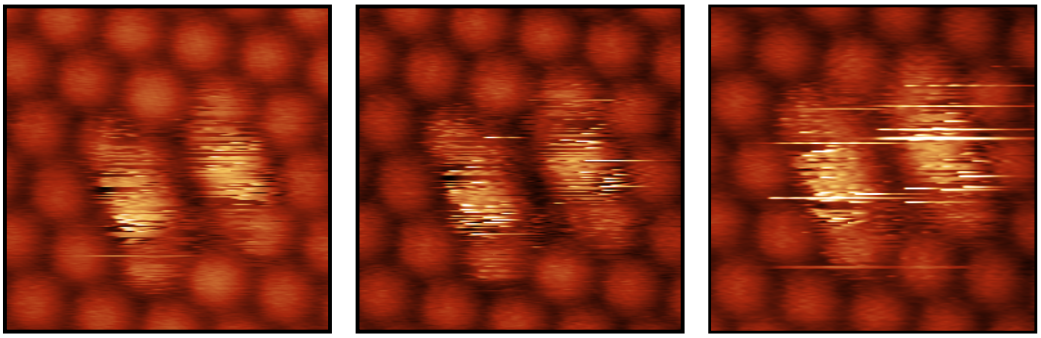

(a) U_S=-1.2 V (b) U_S=-1.6 V (c) U_S=-2.0 V

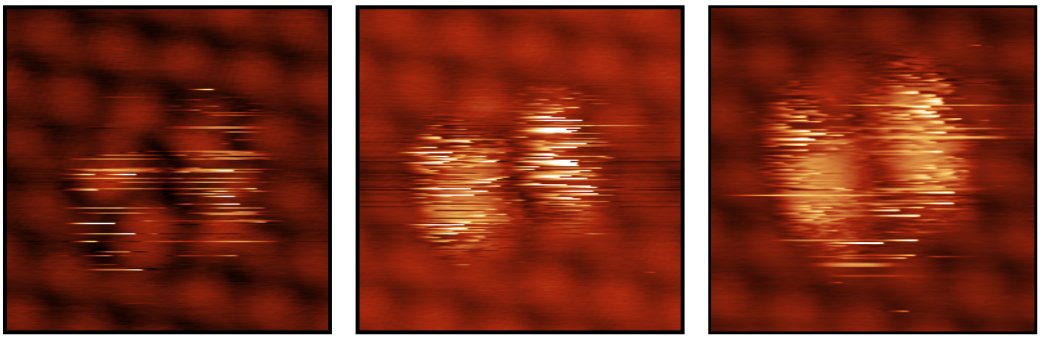

(d) U_S=1.2 V (e) U_S=1.6 V (f) U_S=2.0 V

Figure 6.6: Voltage dependent STM images of fuzzy imaged H_2Pc in filled (first row) and empty (second row) states. The filled state image was taken in the forward scan and empty state image in the backward scan. Images were taken in a constant current mode with tunneling current I_T=0.3 nA. Scanning speed: 77 nm/s. Image size: 2.4×2.4 nm^2.

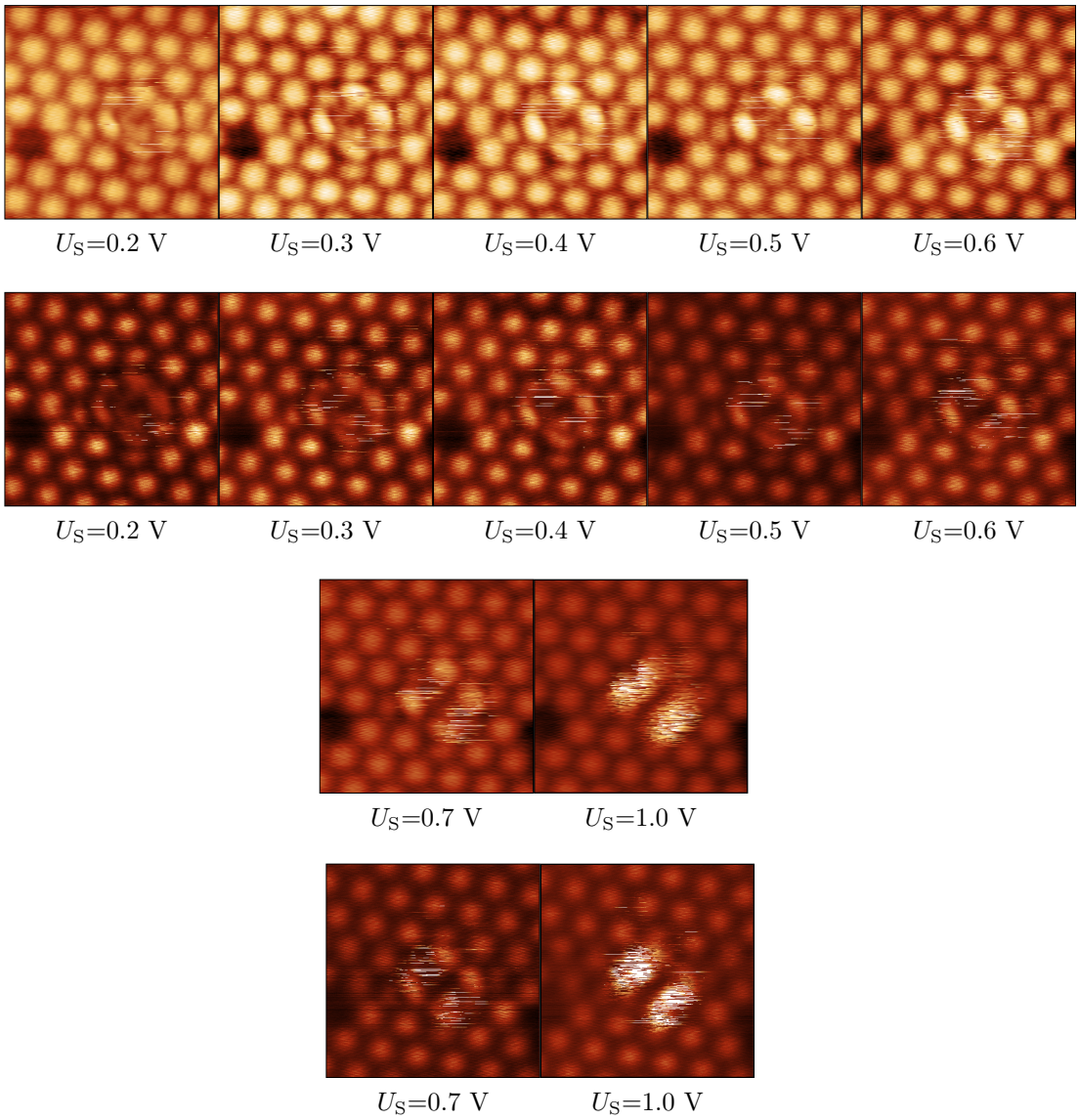

Figure 6.7: Voltage dependent STM images of fuzzy imaged H_2Pc in empty states. First and third row – constant current mode I_T=0.1 nA in a forward scan, second and fourth row – corresponding images at the same sample bias taken in constant hight mode in a backward scan. Scanning speed: 32 nm/s. Image size: 3.9 × 3.9 nm^2.

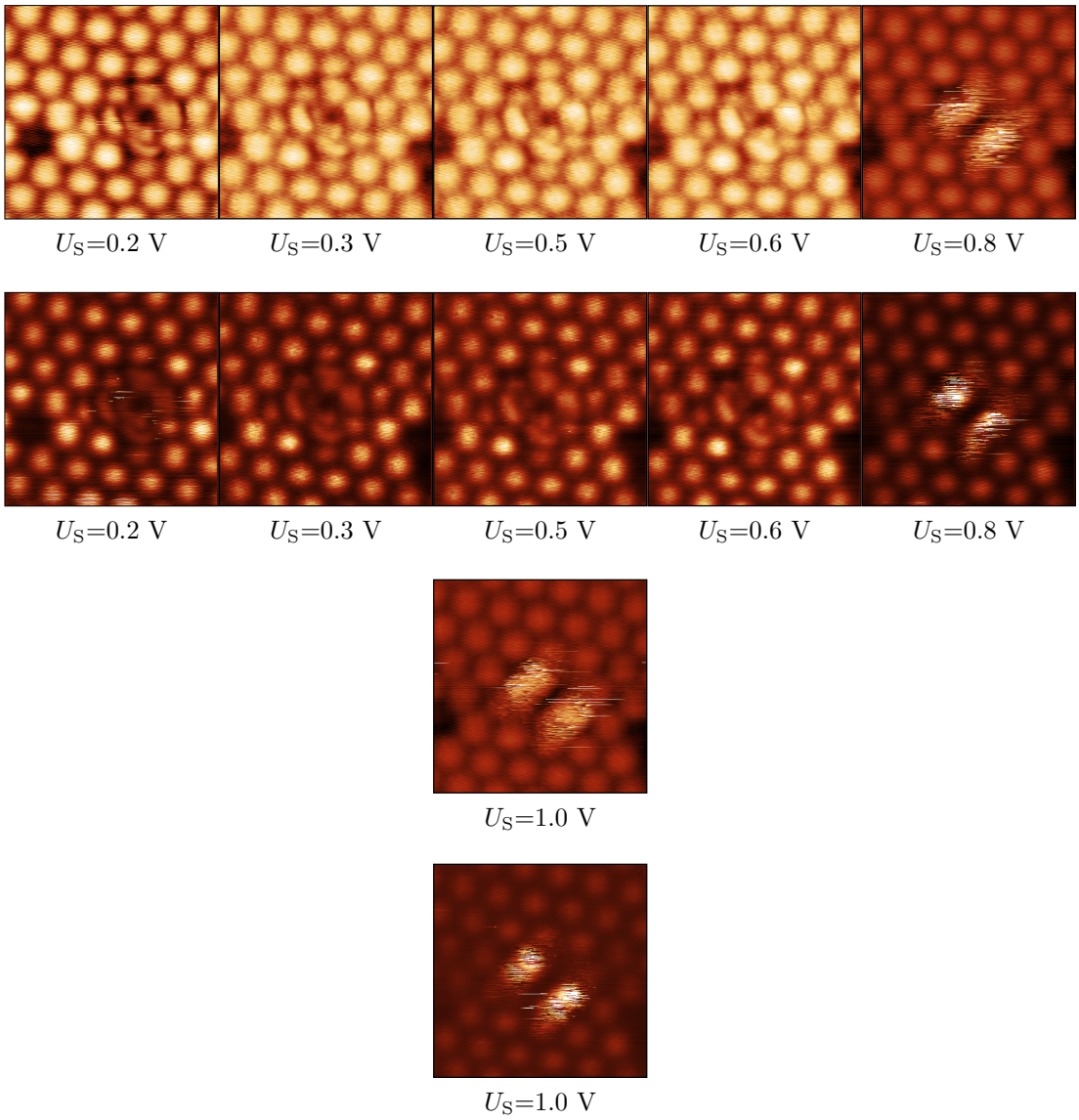

Figure 6.8: Voltage dependent STM images of fuzzy imaged H_2Pc in filled states. First and third row – constant current mode I_T=0.1 nA in a forward scan, second and fourth row – corresponding images at the same sample bias taken in constant hight mode in a backward scan. Scanning speed: 32 nm/s. Image size: 3.9 × 3.9 nm^2.

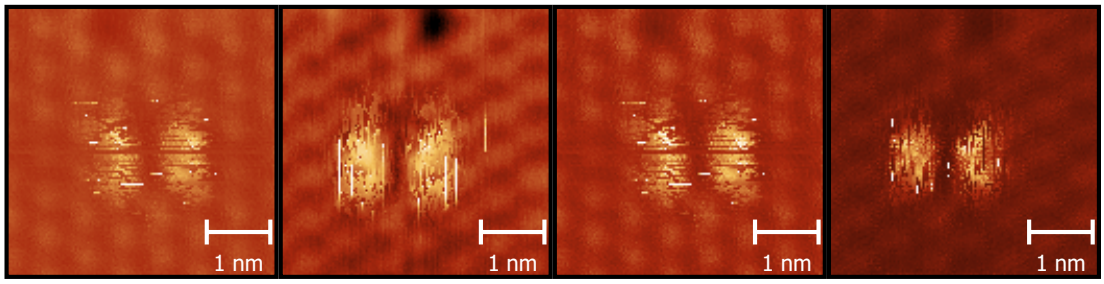

(a) H_2Pc, U_S=-2 V (b) H_2Pc, U_S=-2 V (c) H_2Pc, U_S=-2 V (d) H_2Pc, U_S=-2 V

Figure 6.9: Influence of scanning parameters on "fuzzy" molecule appearance. I_T=0.3 nA and scanning speed 13 nm/s. (a) Constant current mode, forward scan. (c) Constant height mode, backward scan.(b) Constant current mode, image acquired in the top-down (forward) movement of the tip. First line is on right and last line on the left. (d) Constant height mode, image acquired in the down-top (backward) movement of the tip. First line is on the right and last line on the left.

6.6 Comparison of 3 types of phthalocyanines adsorbed on a Si double defect

Comparison of the appearance of different phthalocyanine molecules adsorbed on a Si-substitutional double defect with each other and with the real size ball structural model can give us a better idea of the adsorption configuration. Based on the STM images we can assume that the $F_{16}CuPc$ molecule which does not appear fuzzy sits on the double defect in flat-lying configuration with orientation depicted in Fig. 6.10h. The fuzzy imaged F_8CuPc and H_2Pc would probably have the lobes similar to the $F_{16}CuPc$ but apart from that exhibit some dynamics that results in a fuzzy behaviour.

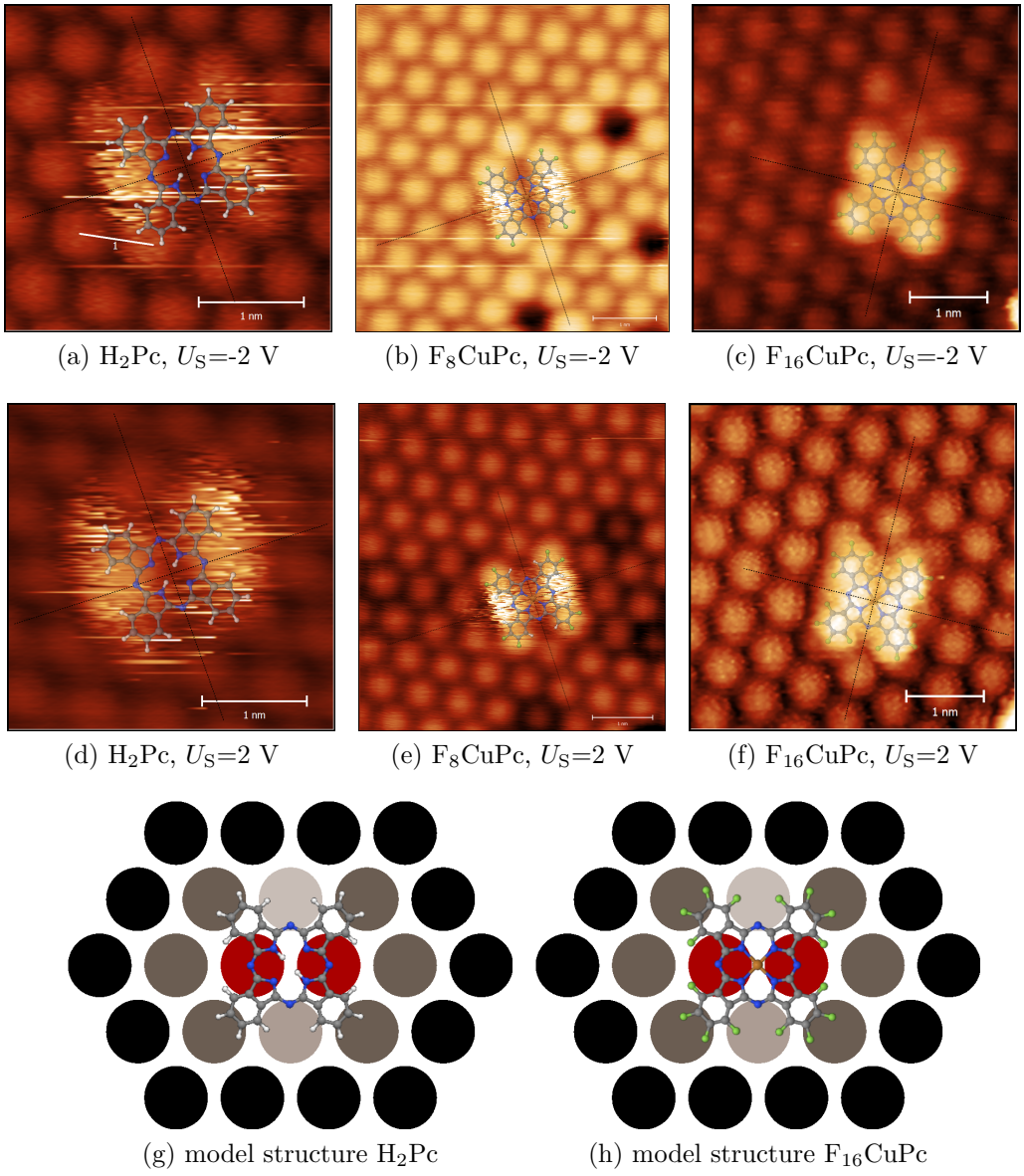

(a) H_2Pc, U_S=-2 V (b) F_8CuPc, U_S=-2 V (c) $F_{16}CuPc$, U_S=-2 V

(d) H_2Pc, U_S=2 V (e) F_8CuPc, U_S=2 V (f) $F_{16}CuPc$, U_S=2 V

(g) model structure H_2Pc (h) model structure $F_{16}CuPc$

Figure 6.10: Comparison of 3 types of fuzzy imaged phthalocyanines adsorbed on Si-substitutional double defect. Real-size structural model of the molecule is superimposed on the STM image. Intersection of dashed lines determines the centre of the molecule and the centre of the double defect. The double defect is in the vertical direction along the dashed line. $F_{16}CuPc$ was measured by Mgr. Karel Majer [65]. (g,f) Proposed orientation of the fuzzy imaged H_2Pc and the adsorption model for the $F_{16}CuPc$ molecule respectively on the double defect. Si-substitutional double defect atoms are red, Sn neighbourhood with one Si neighbour is grey and with two neighbours is light grey. Unperturbed Sn atoms are black.

6.7 H_2Pc on In/Si(111)–($\sqrt{3} \times \sqrt{3}$)

In one of our measurements, adsorption of H_2Pc on the In/Si(111)–($\sqrt{3}\times\sqrt{3}$) was probed. No "fuzzy" objects were recognized. This is interesting since CuPc molecules (also "fuzzy" on double defects on the Sn/Si(111)) exhibit fuzzy behaviour on the In/Si(111)–($\sqrt{3}\times\sqrt{3}$). According to the symmetry, four-lobe molecule in right bottom of the figure 6.11 could sit on the double defect, but we have no evidence for it.

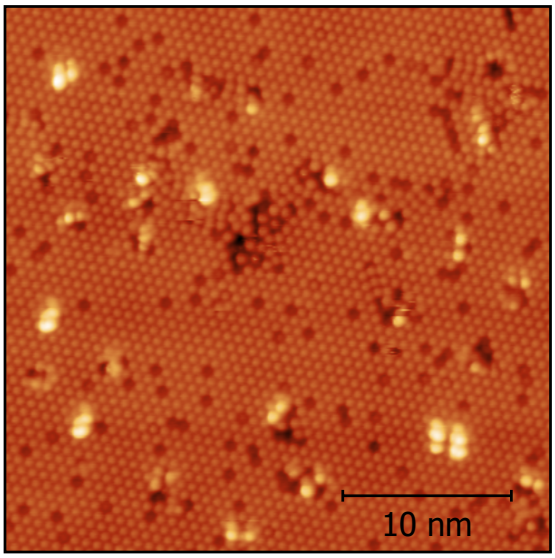

Figure 6.11: Empty state image of the In/Si(111)–($\sqrt{3}\times\sqrt{3}$) with 0.05 ML of H_2Pc molecules. Forward scan, sample bias voltage U_S=2 V and I_T=0.1 nA. Tip is not metallic and is slightly doubled (ghosts of features are visible in the direction towards top of the image). No objects like "fuzzy" molecules were recognized during the measurement.

6.8 Electronic structure of molecules – dI/dV spectra

$\mathrm{d}I/\mathrm{d}V$ spectra of molecules were measured in order to analyse how the adsorption of molecules on defects influences their LDOS. During every measurement, $\mathrm{d}I/\mathrm{d}V$ spectra on clean parts of the Sn/Si(111)–($\sqrt{3}\times\sqrt{3}$) reconstruction were measured as a reference and compared with already published results in Fig. 3.5 and unpublished results from doc. Pavel Sobotík [65].

One can see that the energy levels of observed peaks on the Si-substitutional defect and the clean Sn surface roughly correspond to [65] measurement. From the LDOS spectra of H_2Pc molecule with three-lobe appearance 6.14 one can estimate the HOMO value as (-0.2 ± 0.1) eV and the LUMO as $(1.2 \pm 0.1$ eV with respect to the Fermi level. In case of the F_8CuPc (see Fig. 6.15c) the HOMO can be estimated as (-1.5 ± 0.3) eV and the LUMO as (1.5 ± 0.3) eV. There are no states in the gap which correspond more to the isolated molecule [47]. As seen during the scanning, the molecule was weakly bound to the surface and probably did not change much its electronic structure when adsorbed on the surface. We were not able to perform STS using lock-in technique on "fuzzy" molecules since the sudden changes of the tunneling current with rate comparable to a period of lock-in detection degrade the $\mathrm{d}I/\mathrm{d}V$ curve.

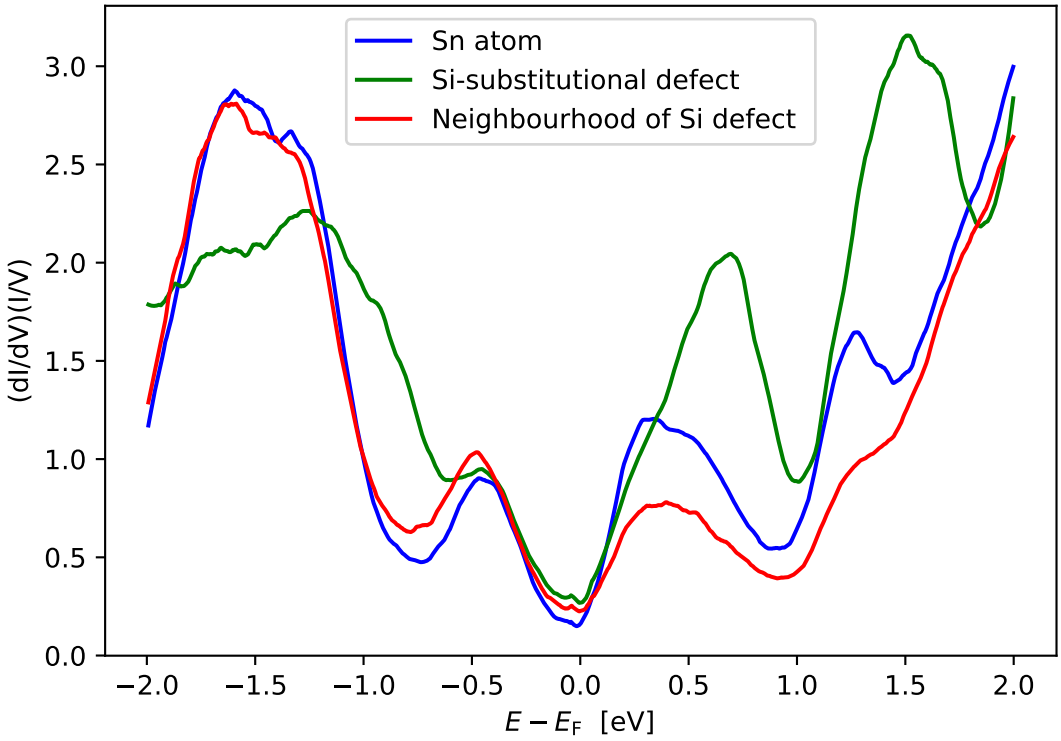

(a) normalized $\mathrm{d}I/\mathrm{d}V$

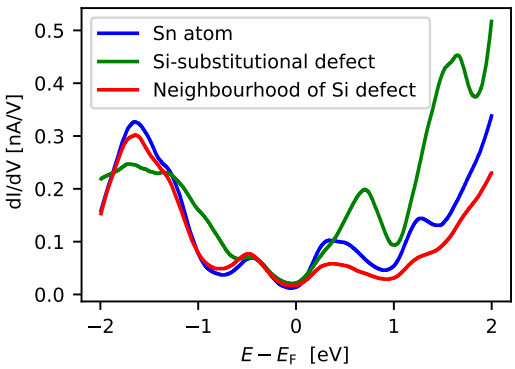

(b) $\mathrm{d}I/\mathrm{d}V$

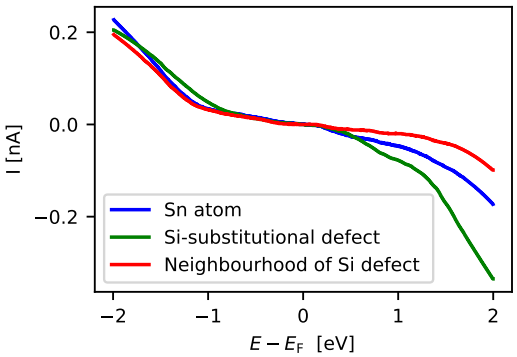

(c) I-V

Figure 6.12: Spectra of the Sn/Si(111)–($\sqrt{3}\times\sqrt{3}$) surface.

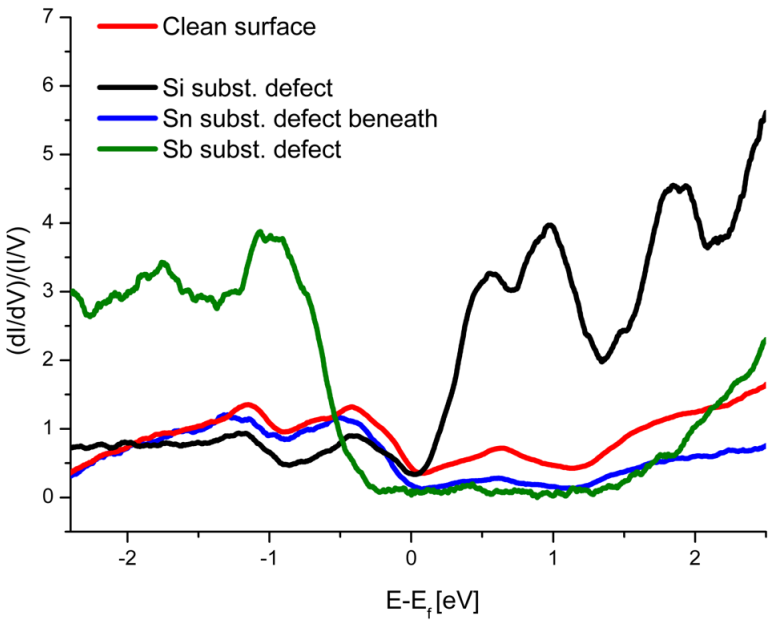

Figure 6.13: Spectra of the Sn/Si(111)–($\sqrt{3}\times\sqrt{3}$) surface measured by doc. Pavel Sobotík [65].

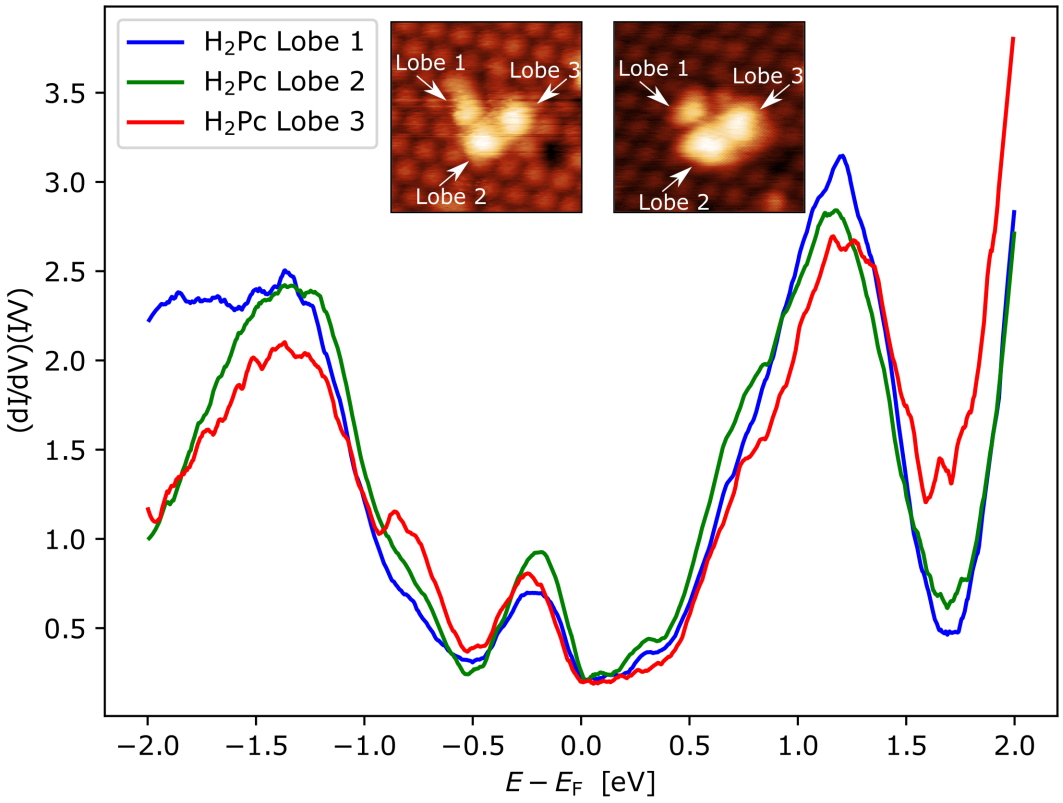

(a) normalized dI/dV

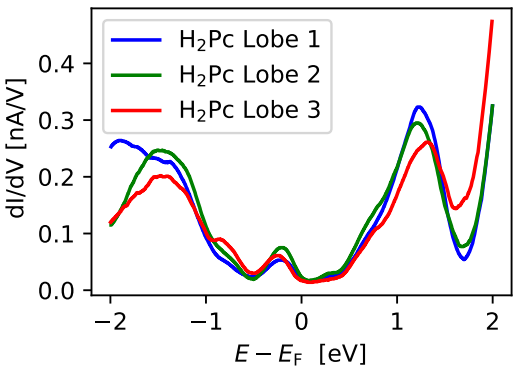

(b) dI/dV

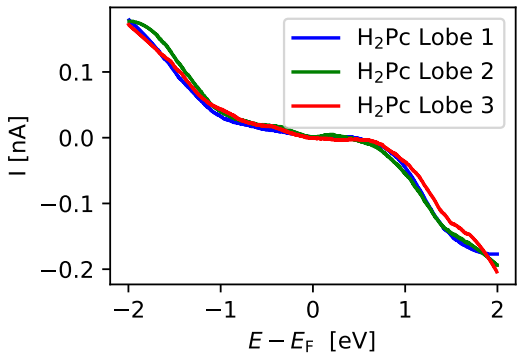

(c) I-V

Figure 6.14: Spectra of a H_2Pc molecule on the Sn/Si(111)–($\sqrt{3}\times\sqrt{3}$). Molecule sits probably on a single Si-substitutional defect (see inset in (a) - left U_S= –2 V, right U_S= +2 V)

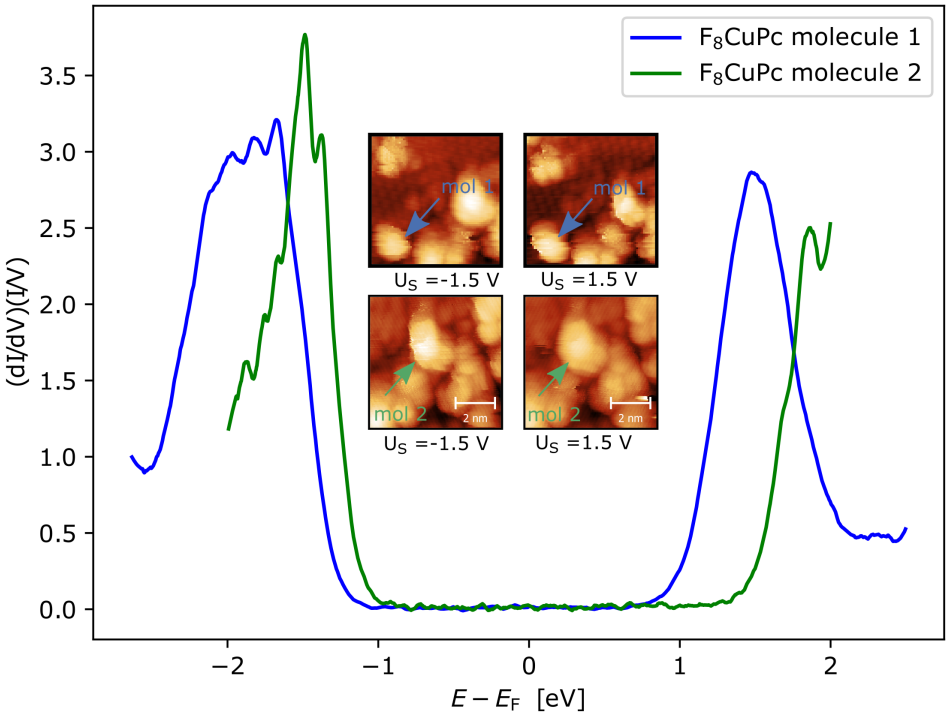

(a) normalized $\mathrm{d}I/\mathrm{d}V$

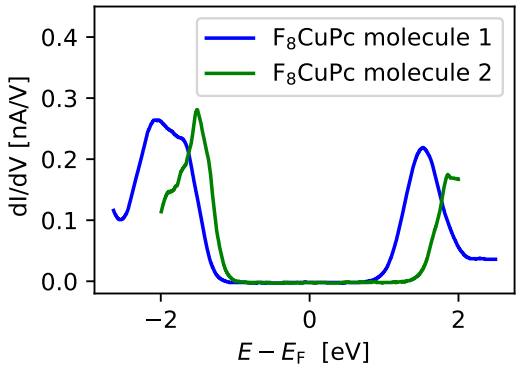

(b) $\mathrm{d}I/\mathrm{d}V$

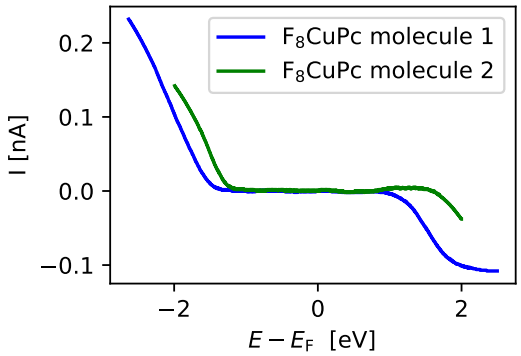

(c) I-V

Figure 6.15: Spectra of two F_8CuPc molecules on the Sn/Si(111)–($\sqrt{3}\times\sqrt{3}$). STS was performed after deposition of 1 ML of F_8CuPc molecules. Molecules grow without any order and form undistinguishable clusters.

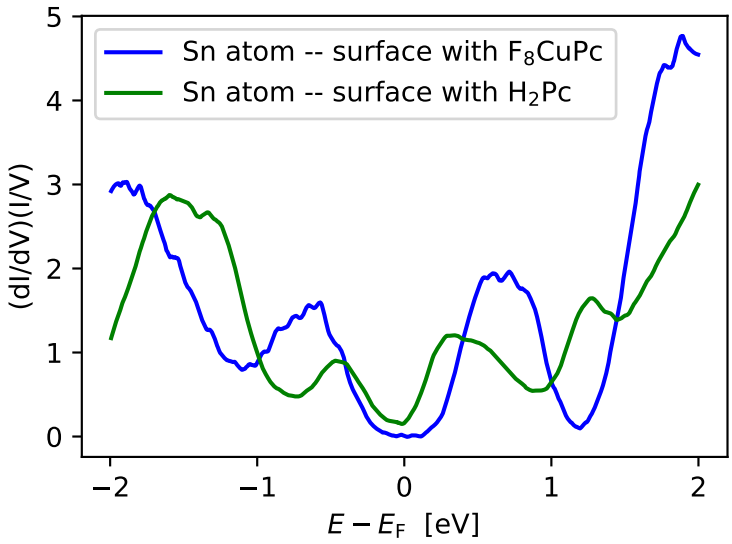

Figure 6.16: Spectra of the shining Sn/Si(111)-($\sqrt{3}\times\sqrt{3}$) surface under the disordered molecular layer (see inset in 6.15a) compared with the spectra in fig. 6.12. A small gap around the Fermi level indicate that tip is not perfectly metallic.

6.9 Fluctuations of tunneling current above a "fuzzy" molecule

From the STM images we saw that molecules on a Si-substitutional double defect exhibit fuzzy behaviour. In order to analyse the fuzzy behaviour more deeply, time series of tunneling current above the molecule was measured. Positions over the lobes of the phthalocyanine molecules that appear fuzzy (see Fig. 6.18) were chosen for acquiring the series. Acquired series in most of the cases had two dominant values of tunneling current with various noise level (see Fig. 6.17). We also acquired time series over the centre of molecule with no dominant and resolvable values of tunneling current. This confirms no observable fuzzy behaviour from STM images. The shown data were processed from measurements on two different H_2Pc molecules and one F_8CuPc molecule. In order to figure out, how the

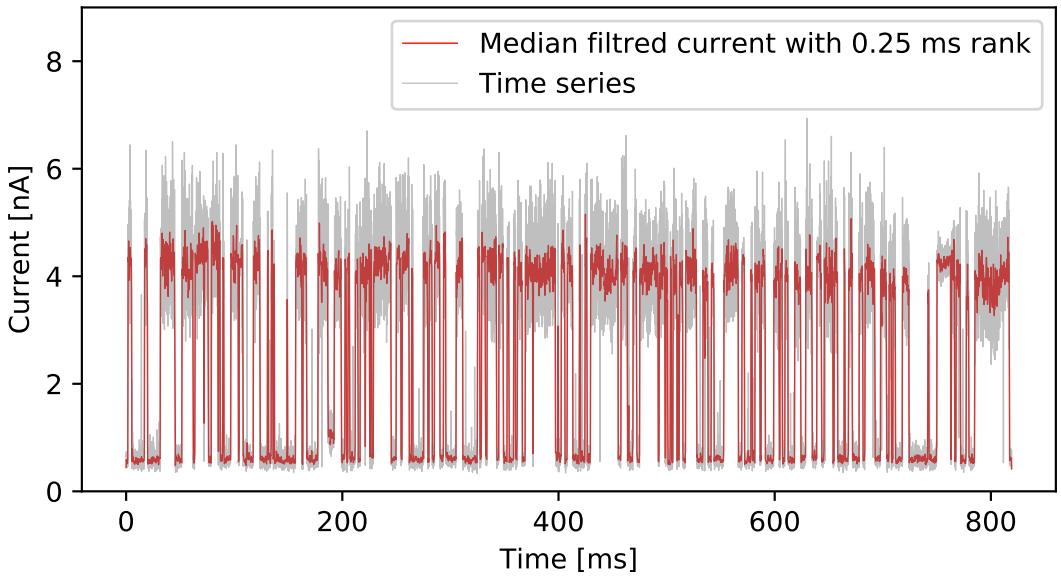

(a)

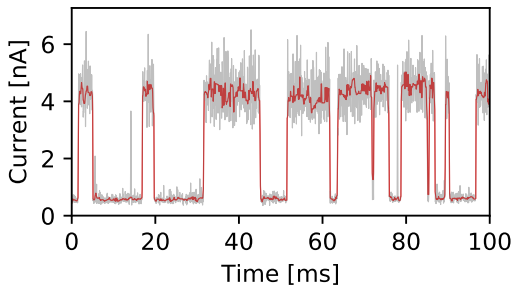

(b)

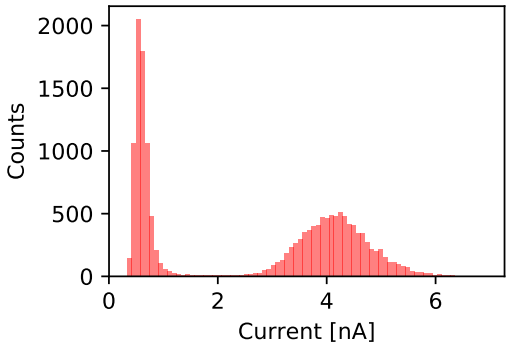

(c)

Figure 6.17: Illustration of time series of tunneling current with two state fluctuations acquired above "fuzzy" H_2Pc at tip bias voltage 2 V a) Series of length 819 ms plotted together with median filtered current. b) 100 ms inset of a). c) Histogram of current values showing the dispersion of both states.

fuzzy imaged H_2Pc molecule behaves, we divide the positions where time series was acquired into *centre of lobe* and *periphery of lobe* (see Fig. 6.18). It can be seen from the graphs that at negative tip bias voltage (empty states) mean lifetime of the fuzzy molecule in the low and the high state is noticeably shorter than for positive tip bias voltages. There is no evidence of influence of mean tunneling current of given state (tip height) on mean lifetime of given state. Also the difference between mean lifetimes of the low and the high state for given time series has no significant trend in the case of H_2Pc molecules (see Tab. 6.2). This corresponds to the graph showing fractional population of states in the low and the high state that is in total more or less equal 6.19. No significant difference is found between time series acquired above *centre of lobe* or above *periphery of lobe*. Since no current or position dependence was observed, average values of mean lifetimes and fractional population were calculated with respect to the tip bias voltage and given state and are summarized in Tab. 6.2.

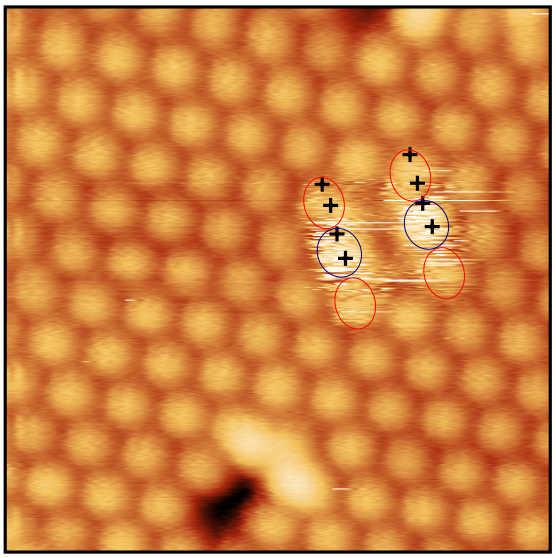

Figure 6.18: Illustration of positions (black crosses) where time series were acquired. For analysis, two inequivalent positions above the H_2Pc molecule are considered with respect to the two-fold rotational symmetry of the fuzzy molecule appearance. *Centre of lobes* are points in the blue ellipses and *periphery of lobes* are points in the red ellipses.

molecule	U_t [V]	τ_{low} [ms]	τ_{high} [ms]	FP low	FP high	n
H_2Pc m. 1	2	6.6 (4.9, 9.0)	6.0 (5.0, 7.0)	0.51 ± 0.05	0.49 ± 0.05	16
	1.6	7.8 (6.0, 10.3)	6.7 (5.0, 9.0)	0.54 ± 0.09	0.46 ± 0.09	11
	1.2	6.8 (5.3, 8.8)	8.3 (7.5, 9.3)	0.50 ± 0.08	0.50 ± 0.08	4
	−2	2.9 (2.1, 4.1)	3.9 (2.2, 7.0)	0.45 ± 0.13	0.55 ± 0.13	13
H_2Pc m. 2	2	9.1 (7.3, 11.3)	10.5 (8.1, 13.7)	0.47 ± 0.10	0.53 ± 0.10	18
	1.2	9.2 (7.8, 11.0)	13.5 (10, 18)	0.41 ± 0.11	0.59 ± 0.11	7
	−2	3.5 (2.8, 4.2)	3.6 (2.4, 5.4)	0.49 ± 0.10	0.51 ± 0.10	5
F_8CuPc	2	6.2 (2.4, 16.3)	5.8 (2.9, 11.6)	0.60 ± 0.14	0.40 ± 0.14	21

Table 6.2: Summary of calculated mean lifetimes τ and fractional population (FP) of both low and high states sorted according to tip bias voltage U_t. The lifetime values are calculated as an exponential of average of logarithm of lifetimes from n measurements $\exp(\frac{1}{n}\sum_i^n \ln(\tau_i))$ and its error is expressed as a confidence interval in parentheses (border points of the interval are calculated as $\exp(\frac{1}{n}\sum_i^n \ln(\tau_i) \pm \sigma)$ where sigma is a standard deviation of the $\ln(\tau_i)$ data set). The FP values are averages from n measurements and their errors are taken as a standard deviation.

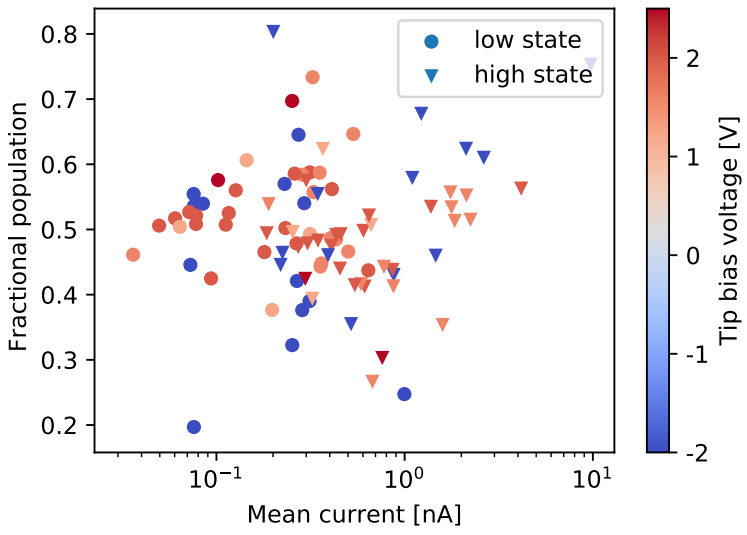

Figure 6.19: Fractional population of states for a fuzzy H_2Pc molecule on the Sn/Si(111)–$(\sqrt{3} \times \sqrt{3})$. Time series taken at tip bias voltages: -2, 1.2, 1.6, 2.0 and 2.5 Volts.

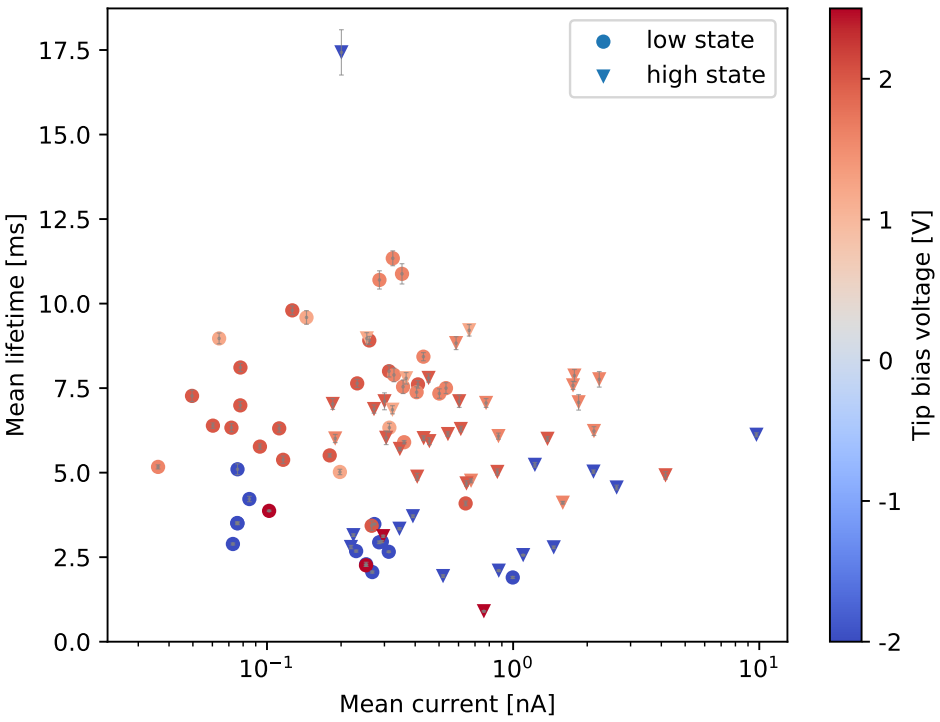

Figure 6.20: Mean lifetime of states for fuzzy H_2Pc molecule on the Sn/Si(111)–$(\sqrt{3} \times \sqrt{3})$. Time series taken at tip bias voltages: -2, 1.2, 1.6, 2.0 and 2.5 Volts.

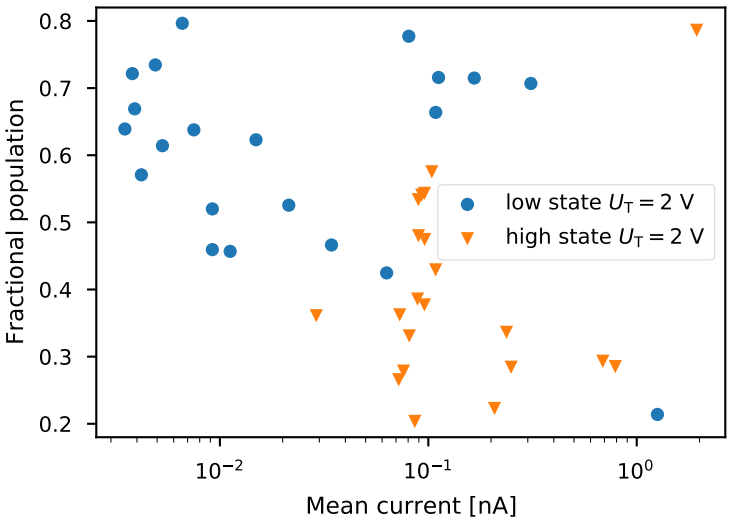

Figure 6.21: Fractional population of states for a fuzzy F_8CuPc molecule on the Sn/Si(111)–$(\sqrt{3} \times \sqrt{3})$. Time series taken at tip bias voltage 2 V.

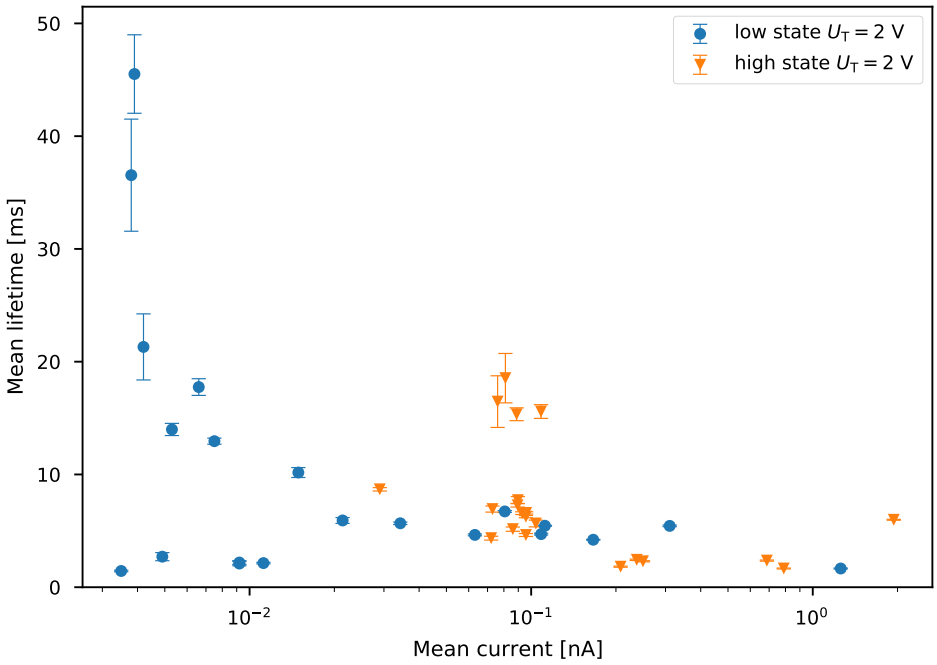

Figure 6.22: Mean lifetime of states for a fuzzy F_8CuPc molecule on the Sn/Si(111)–($\sqrt{3} \times \sqrt{3}$). Time series taken at tip bias voltage 2 V.

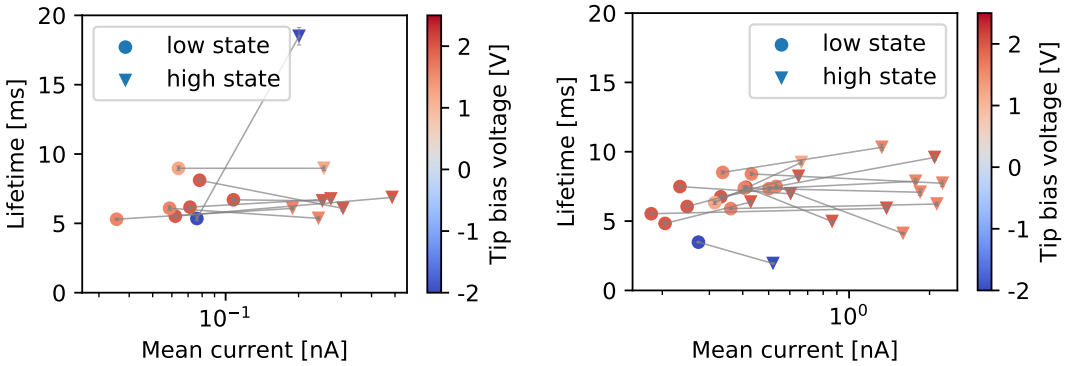

(a) centre of lobes low setpoint current

(b) centre of lobes high setpoint current

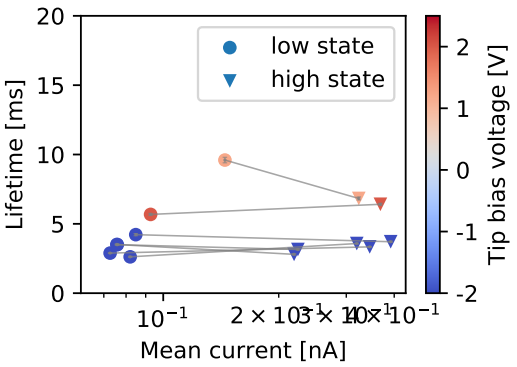

(c) periphery of lobes low setpoint curreent

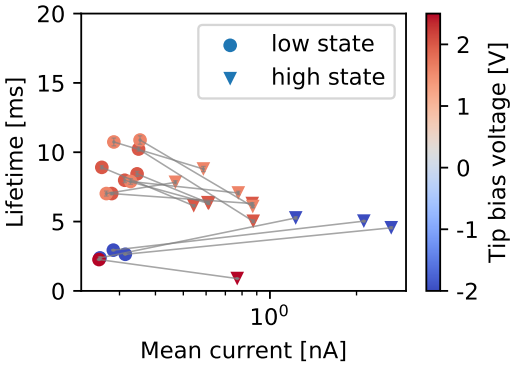

(d) peripehery of lobes high setpoint current

Figure 6.23: Mean lifetime of states for a fuzzy H_2Pc molecule on the Sn/Si(111)–$(\sqrt{3} \times \sqrt{3})$. Time series taken at tip bias voltages: -2, 1.2, 1.6, 2.0 and 2.5 Volts. Data for the molecule 1. Two states apparent in one series are linked together with the grey line.

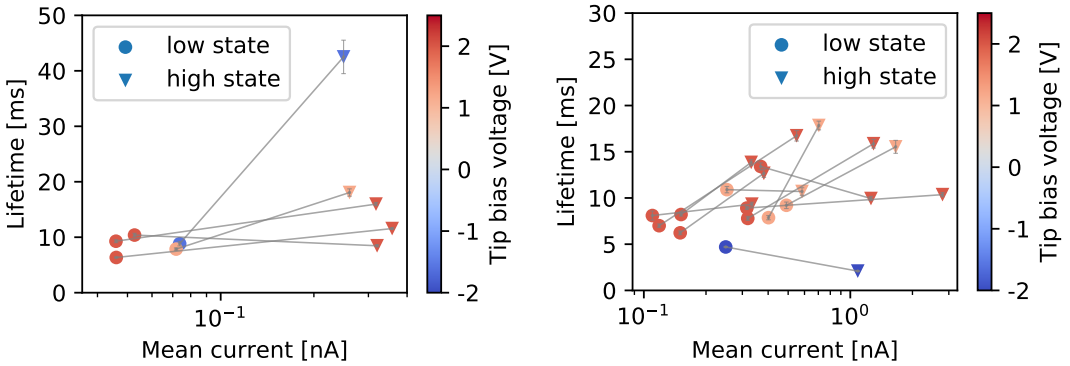

(a) centre of lobes low setpoint current

(b) centre of lobes high setpoint current

(c) periphery of lobes low setpoint current

(d) peripehery of lobes high setpoint current

Figure 6.24: Mean lifetime of states for a fuzzy H_2Pc molecule on the Sn/Si(111)–$(\sqrt{3}\times\sqrt{3})$. Time series taken at tip bias voltages: -2, 1.2, 1.6 and 2.0 Volts. Data for the molecule 2. Two states apparent in one series are linked together with the grey line.

7. Discussion

STM images provide us with 3 types of information about the surface: topography, electronic structure and the dynamics on the surface. It is possible to separate the information about electronic structure from topography e. g. by measurement on LDOS of the molecule by means of STS.

LDOS measurement

Free-standing phthalocyanine molecule has four-fold rotational symmetry and the HOMO-LUMO gap is around 2-2.2 eV [47] (see Fig. 4.2) for the phthalocyanines used in our thesis. These values were calculated by DFT. The presence of fluorine substituents determines only the energy level of both HOMO and LUMO with respect to the Fermi level but not the gap between them. In the case of the adsorption of phthalocyanines on surfaces and their mutual strong interaction – chemisorption, the energy levels of molecules are perturbed and broadened, the imaging of the molecule is changed and its 4-fold rotational symmetry is not visible. From LDOS spectra measured on the H_2Pc molecule (see Fig. 6.14), it is obvious that values of the HOMO and the LUMO change in comparison with a free-standing molecule, whereas in the case of the weakly adsorbed F_8CuPc (see Fig. 6.15c) the HOMO and LUMO energy values as well as the pronounced gap between them correspond better to the free-standing molecule. Unfortunately, neither lock-in technique nor I-V numerical derivative can be used to measure spectra on fuzzy imaged molecules. Even though we had measured the I-V curve, careful separation of both states and subsequent differentiation was not possible from our measurements. Previous measurements of I-V [65] showed the splitting of the curve for the low and the high state, nevertheless the splitting was apparent only at large enough voltages (> 1.5 V) and the curve was not convenient for differentiation. The only information we can get about the electronic structure is the integral value of the density of states present in voltage dependent images.

Model of fuzzy imaged phthalocyanines

Fuzzy imaging was observed on a Si-substitutional double defect on the Sn/Si(111)–($\sqrt{3}\times\sqrt{3}$) reconstruction in the case of the CuPc [65], H_2Pc and F_8CuPc but not in the case of the $F_{16}CuPc$. It was also observed on the In/Si(111)–($\sqrt{3}\times\sqrt{3}$) in the case of the CuPc molecule but not in the case of the H_2Pc. If we limit ourselves only on the tin reconstruction, we can say that STM images of "fuzzy" CuPc look similar to "fuzzy" H_2Pc ones. This is in agreement with the images based on DFT calculations which also show similar charge distribution in the centre of phthalocyanine molecule upon change from CuPc to H_2Pc 4.2. However, the charge distribution of copper phthalocyanines with 8 or 16 fluorine substituents is changed which results in their larger appearance in STM in comparison with the non-fluorinated ones mainly due to the longer fluorine-carbon bond.

From all possible effects than can result in two state fluctuations of tunneling current at room temperature the tautomerization of inner hydrogen atoms can be ruled out since the fluctuations were measured both on hydrogen and copper

phthalocyanines. The fuzzy image of a molecule has reduced two-fold rotational symmetry and along the axis a_{dd} no fluctuations are recorded which disfavours rotation of the molecule around its axis as a source of the fuzzy imaging behaviour. According to the symmetry of the problem, we present two explanations of the fluctuations which we think are the most probable ones. Both explanations consider a motion of the molecule in a double-well potential on the surface – hopping between the two minima (see Fig. 7.1) as an origin of the measured current fluctuations. The molecular orbitals change their position (between two possible ones) under the tip and two discrete levels of tunneling current are measured.

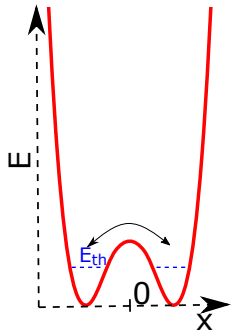

Figure 7.1: Illustration of the double-well potential in the Energy-distance diagram as the model for "fuzzy" molecule adsorption. Thermal energy E_{th} increases the molecular hopping probability, same level of both minima corresponds to the fractional population of both states equal to 0.5.

The first possible motion is a vertical overturn of the molecule over the axis connecting double defect atoms (type X overturn). The two neighbouring lobes stick out into the free space in the z-coordinate while the two opposite lobes are fixed to the surface – this is one state – and vice versa in the other state. The switching between the states is caused by the repeated overturning and results in tunneling current fluctuations. In the area over the double defect therefore no fluctuations appear since the centre of the molecule is at the same height in both states. This explanation would also correspond to the observed capture of the CuPc molecule always in one and then in the other state (see Fig. 4.6). Nevertheless, the capture was observed at the tip bias voltage of ± 3 V which indicates unstable conditions. The capture itself could be induced dominantly by a strong electric field which traps the molecule in a new state that is not observed during the regular measurements. The presence of other adsorption positions (or rather capture positions) of phthalocyanines has probably been already observed after an unsuccessful attempt to remove the molecule from the double defect by the gradual tip approach to the surface in the constant height mode. We cannot exclude that the local arrangement of the surface atoms was not changed and the double defect was not removed during a high voltage pulse or a close tip-sample distance.

The other possibility of the molecular motion is its translation along the axis a_{dd} with the centre of the molecule closer to one or to the other Si atom in the two states. The fuzzy image of the molecule then should appear elongated in the direction of the axis a_{dd}. The path of the motion can even be relatively small, circa 0.1 nm, yet the resulting change of the electronic structure between the two mirror-symmetric adsorption positions can be significant and can result in a large

change in the tunneling current. In the area over the double defect probably no orbitals which can be observed as fuzzy are present. The origin of the non-fuzzy behaviour of F_{16}CuPc on the double defect can be explained by the fact that for the large molecule with all 16 outer positions substituted by fluorines, the potential energy relief changes from the double-well shape to a single-well shape. One cannot exclude the unlikely case in which the barrier between the minima of the double well is only reduced, the hopping is accelerated and we see a time-averaged image in STM. In order to shed some light on the problem it would be necessary to image the capture in both states separately otherwise we can only state hypotheses.

Influence of the tip on the fuzzy behaviour of molecules

An important question arises: How much is the fuzzy behaviour influenced by the presence of the tip? The applied tip bias voltage causes an electric field between the tip and the sample. If we consider the tip radius of curvature of more than 50 nm, in first approximation, we can consider the electric field close to the tip apex as homogeneous given by

$$E = \frac{U}{d} \tag{7.1}$$

where U is the bias voltage and d the tip-sample distance. If we imagine that the typical tip-sample distance d is approximately 0.5 nm and it changes only slowly with the change of the current due to the logarithmic dependence, the voltage change will be dominant for the magnitude of the electric field due to their linear dependence. If we assume that the molecule on a surface has certain non-zero permanent dipole moment $\vec{p}$ (we neglected higher order moments), its potential dipole energy in the homogeneous electric filed can be written as

$$E_{\mathrm{d}} = -\vec{p} \cdot \vec{E} \tag{7.2}$$

This energy can be compared to the thermal energy

$$E_{\mathrm{th}} = k_{\mathrm{B}} T \tag{7.3}$$

if we know the exact value of the dipole moment e. g. from DFT [70]. If the absolute value of the dipole energy is smaller than the thermal energy, thermal fluctuations will be dominant and the electric field will have negligible effect on the molecule under the tip. In the latter case, when the dipole energy is higher than the thermal energy, the double-well potential can be deepened and the switching rate can be decreased in one bias voltage polarity and vice versa in the other polarity of bias voltage. This corresponds to the results of analysis of tunneling current fluctuations which showed that the mean lifetime of states is lower (frequency is higher) for negative tip bias voltage and the mean lifetime of states is higher for positive tip bias voltages in case of the H_2Pc molecule. This observation therefore indicates that the molecule has a non-zero permanent dipole moment.

Another key result of time series analysis is that we cannot see a dependence of mean lifetime and fractional population of states on the position of the tip above the molecule, where time series was acquired. If we imagine the presence

of the tip with the applied bias voltage between the tip and the sample as a perturbation of the double-well potential landscape, we would expect deepening of one of the minima in *periphery of lobe* position which should appear in fractional population inequality of both states. The possible explanation of this problem is as follows: Due to the large tip radius of curvature in comparison with the size of the phthalocyanine molecule the inhomogeneity of electric field in the molecule area of 1.4×1.4 nm^2 is so small that in any position of the tip above the molecule mutual energy positions of the minima of the double well do not differ in the way detectable in time series analysis. If any asymmetric perturbation of the double-well potential is caused, we do not see it since in our data set of measurements in different positions the fractional populations of both states are averaged after calculation of their mean values. In summary, time series analysis of tunneling current fluctuations above fuzzy imaged phthalocyanine molecules revealed that the fuzzy behaviour is influenced by the presence of the tip, but this is not the main reason of the fuzzy behaviour which we think is a thermally activated hopping in the double-well potential.

Disappearance of tunneling current fluctuations in low bias STM images

From the voltage dependent images of "fuzzy" molecules, it is evident, that there is a threshold bias voltage of $\pm$ 0.7 V of fuzzy appearance for both H_2Pc and F_8CuPc below which fluctuations are not imaged. It can be caused either by a disappearance of voltage activated fluctuations or by an absence of states responsible for fuzzy imaging on energy levels in the gap between -0.7 V and 0.7 V sample bias voltage. If we knew the LDOS of "fuzzy" molecules the question would be easier to answer, nevertheless, we prefer the former theory. The activation threshold bias voltage of fluctuations should have either positive or negative value but not two values in both polarities if we consider that the molecule has a permanent dipole moment. Most probably, we do not see the fluctuations only on certain energy levels in the STM. This can be explained in terms of a resonant tunneling through the molecule adsorbed on a surface. Let us imagine that the molecule has discrete levels in the "vacuum gap" between the tip and the sample. If those levels are on the energy level of tunneling (Fermi level of the tip or the sample) they can mediate the tunneling and effectively reduce the barrier width. The current in this case is much higher than in the case of tunneling through the molecule on the level with no states, because the barrier width is the tip-sample distance which is larger than the tip-molecule distance.

The visibility of fluctuations in the STM image depends on the orbital distribution change in space at given energy (bias voltage) and if the change is negligible, we do not see the fluctuations.

Undesired effects at tunneling junction

When interpreting the results the tip quality and stability in time during the measurements should be taken into account. It is important to keep in mind, that the tip height is controlled by a feedback loop and depends on the preset tunneling current. If the preset current is too high and the absolute value of the

bias voltage is scaled down, it is a common phenomenon that the tip resolution is lost – the feedback loop approaches the tip towards the surface too close in order to maintain the desired tunneling current and the atomic manipulation between the tip and the surface occurs. Scanning at low biases requires low tunneling current and a clean metallic tip as well as the surface without a gap on the bias voltage used which is sometimes difficult to guarantee (the Sn/Si(111)–($\sqrt{3}\times\sqrt{3}$) meets the condition because it has no gap). The interpretation of STM images taken at low bias voltages is therefore tricky since the influence of atomic forces can be never excluded. This is valid also for large voltages (generally more than 2 V in both polarities) due to the large electric field induced, especially when probing "fuzzy" molecules. It is a task for the experimental physicist to evaluate which information is reliable and perform ideally reproducible experiments if the obtained results raises doubts.

Conclusion

Adsorption of H_2Pc and F_8CuPc phthalocyanines was probed on the Sn/Si(111)–($\sqrt{3}\times\sqrt{3}$) and the In/Si(111)–($\sqrt{3}\times\sqrt{3}$) reconstruction by means of room temperature STM. At low coverage the phthalocyanine molecules at room temperature adsorb only on Si-substitutional defects of the surfaces. On the Sn/Si(111)–($\sqrt{3}\times\sqrt{3}$) several adsorption configurations of the H_2Pc phthalocyanine were recognized. On the Si-substitutional double defect the adsorbed phthalocyanines are imaged fuzzy in STM. F_8CuPc phthalocyanines also exhibit fuzzy behaviour on the Si-substitutional double defect and adsorb predominantly on these defects. On the In/Si(111)–($\sqrt{3}\times\sqrt{3}$) surface, no fuzzy imaged molecules were recognized which is in contrast with the previous measurements of the CuPc [65] which have shown fuzzy behaviour of the CuPc molecule on both tin and indium passivated silicon surfaces.

Electronic structure of bare metal passivated silicon surfaces was measured by means of STS and compared with previous measurements [65]. Significant agreement with these results was found. Spectra on the strongly adsorbed three-lobe imaged H_2Pc on the Sn/Si(111)–($\sqrt{3}\times\sqrt{3}$) were measured with the same tip as the spectra on the bare surface. The HOMO value of this molecule was estimated as (-0.2 ± 0.1) eV and the LUMO value as (1.2 ± 0.1) eV with respect to the Fermi level. From the spectra on a weakly bound F_8CuPc molecule its HOMO value was estimated as (-1.5 ± 0.3) eV and its LUMO value as (1.5 ± 0.3) eV which corresponds to the free-standing molecule.

We have focused on probing the origin of "fuzzy" molecule appearance. Two dominant values of tunneling current were present in the time series analysis above fuzzy imaged lobes of molecules. This corresponds to the switching of the molecule between two states. The mean lifetime of the states is 8 ms with confidence interval $(5, 14)$ ms for both the low and the high state of the H_2Pc molecule and 6 ms with confidence interval $(3, 16)$ ms for both the low state and the high state of the F_8Pc molecule at 2 V tip bias voltage. For the negative tip bias voltage -2 V, the mean lifetime of both states is half that of the value for positive tip bias voltage. Fractional population of both states is equal for the H_2Pc molecule.

We attribute the fuzzy behaviour of the molecule to the molecular motion in the double-well potential. Either lateral movement along the axis a_{dd} or the type X overturn are in agreement with all the measured data. We assume that the double-well potential is symmetric corresponding to the 0.5 fractional population of both states. We expect that the fluctuations are thermally activated and partially influenced by the electric field between the tip and the sample. We think that the fuzzy imaged phthalocyanine molecule has a dipole moment and an additional energy of the dipole in the electric field deepens or reduces the double well which changes the rate of the fluctuations. In order to clarify the fuzzy behaviour we propose to perform time series analysis at reduced temperatures, from which the activation energy and the frequency prefactor can be determined using the fit of the Arrhenius equation. If the rate decreased with the decreased temperature down to tenths of Hz, the molecule could be captured in a single state in the STM image and its adsorption position could be determined. A DFT

study can also help to resolve the problem.

For potential applications in molecular scale electronics, random switching must be suppressed and ideally the switching should be induced e. g. by voltage pulse and it must be reversible. This could by done by cooling the surface down to sufficiently low temperature.

Fulfilment of the task description

- The first goal was fulfilled. The tin and the indium passivated Si(111) surface with the $\sqrt{3} \times \sqrt{3}$ reconstruction was chosen to be further examined since the adsorption of phthalocyanines on Si-substitutional double defects is an interesting problem in surface physics and other reconstructions were already probed in the Thin Films group.

- Surfaces with well defined amount of defects were successfully prepared.

- The third goal was completely fulfilled and LDOS of surface measured by STS is presented.

- The greatest attention was paid to the fourth goal. The adsorption of phthalocyanines on Si-substitutional double defects was studied and a possible explanation of its fuzzy behaviour in STM images is presented.

- 1 ML coverage of F_8CuPc on the Sn/Si(111)–($\sqrt{3}\times\sqrt{3}$) reconstruction was created and no self-organization of molecules has been observed. Molecules formed undistinguishable clusters on which LDOS was measured and discussed. The monolayer coverage was not further studied since the surface with cluster-like objects is not convenient to study in STM.

Bibliography

[1] Leonhard Grill, Matthew Dyer, Leif Lafferentz, Mats Persson, Maike V Peters, and Stefan Hecht. Nano-architectures by covalent assembly of molecular building blocks. *Nature nanotechnology*, 2(11):687, 2007.

[2] Jia Lin Zhang, Jian Qiang Zhong, Jia Dan Lin, Wen Ping Hu, Kai Wu, Guo Qin Xu, Andrew TS Wee, and Wei Chen. Towards single molecule switches. *Chemical Society Reviews*, 44(10):2998–3022, 2015.

[3] Jong Yeog Son and Hyunwook Song. Molecular scale electronic devices using single molecules and molecular monolayers. *Current Applied Physics*, 13(7):1157–1171, 2013.

[4] Russell Young, John Ward, and Fredric Scire. The topografiner: an instrument for measuring surface microtopography. *Review of Scientific Instruments*, 43(7):999–1011, 1972.

[5] Erwin W Müller. Field ion microscopy. *The Physics Teacher*, 4(2):53–56, 1966.

[6] Chunli Bai. *Scanning tunneling microscopy and its application*, volume 32. Springer Science & Business Media, 2000.

[7] John Bardeen. Tunnelling from a many-particle point of view. *Physical Review Letters*, 6(2):57, 1961.

[8] Bert Voigtländer. *SCANNING PROBE MICROSCOPY.* Springer, 2016.

[9] C Wagner, R Franke, and T Fritz. Evaluation of I (V) curves in scanning tunneling spectroscopy of organic nanolayers. *Physical Review B*, 75(23):235432, 2007.

[10] Kedong Wang, Chun Zhang, Michael MT Loy, and Xudong Xiao. Time-dependent tunneling spectroscopy for studying surface diffusion confined in nanostructures. *Physical review letters*, 94(3):036103, 2005.

[11] J Schaffert, MC Cottin, A Sonntag, H Karacuban, D Utzat, CA Bobisch, and R Möller. Scanning noise microscopy. *Review of Scientific Instruments*, 84(4):043702, 2013.

[12] Kunio Takayanagi, Yasumasa Tanishiro, Shigeki Takahashi, and Masaetsu Takahashi. Structure analysis of Si (111)-7× 7 reconstructed surface by transmission electron diffraction. *Surface science*, 164(2-3):367–392, 1985.

[13] Andrey V. Zotov and Alexander A. Saranin. DAS Model. `http://eng.thesaurus.rusnano.com/wiki/article14156`. Accessed: 2017-05-03.

[14] Werner Kern. The evolution of silicon wafer cleaning technology. *Journal of the Electrochemical Society*, 137(6):1887–1892, 1990.

[15] Sean R. Wagner, Bing Huang, Changwon Park, Jiagui Feng, Mina Yoon, and Pengpeng Zhang. Growth of Metal Phthalocyanine on Deactivated Semiconducting Surfaces Steered by Selective Orbital Coupling. *Phys. Rev. Lett.*, 115:096101, Aug 2015.

[16] Hojin Jeong and Sukmin Jeong. Diffusion of Ag adatom on the H-terminated and clean Si(111) surfaces: A first-principles study. *Phys. Rev. B*, 71:035310, Jan 2005.

[17] J Nogami, Sang-il Park, and CF Quate. Structure of submonolayers of tin on Si (111) studied by scanning tunneling microscopy. *Journal of Vacuum Science & Technology A*, 7(3):1919–1921, 1989.

[18] PJ Estrup and J Morrison. Studies of monolayers of lead and tin on Si (111) surfaces. *Surface Science*, 2:465–472, 1964.

[19] Toshihiro Ichikawa. Structural study of ultrathin Sn layers deposited onto Ge (111) and Si (111) surfaces by RHEED. *Surface science*, 140(1):37–63, 1984.

[20] L Ottaviano, G Profeta, L Petaccia, CB Nacci, and S Santucci. Structural and electronic properties of the Sn/Si (111)-($2\sqrt{3} \times 2\sqrt{3}$) R30° surface revised. *Surface science*, 554(2):109–118, 2004.

[21] C Törnevik, M Göthelid, M Hammar, Ulf O Karlsson, NG Nilsson, SA Flodström, C Wigren, and M Östling. Adsorption of Sn onSi (111) 7× 7: reconstructions in the monolayer regime. *Surface science*, 314(2):179–187, 1994.

[22] B Ressel, C Di Teodoro, G Profeta, L Ottaviano, V Cháb, and KC Prince. Scanning tunneling spectroscopy investigation of the ($\sqrt{3}\times\sqrt{3}$) R30° Sn/Si (1 1 1) α and γ surfaces. *Surface science*, 562(1-3):128–136, 2004.

[23] S. Modesti, L. Petaccia, G. Ceballos, I. Vobornik, G. Panaccione, G. Rossi, L. Ottaviano, R. Larciprete, S. Lizzit, and A. Goldoni. Insulating Ground State of Sn/Si(111)$-(\sqrt{3}\times\sqrt{3})R30°$. *Phys. Rev. Lett.*, 98:126401, Mar 2007.

[24] G. Profeta and E. Tosatti. Triangular Mott-Hubbard Insulator Phases of Sn/Si(111) and Sn/Ge(111) Surfaces. *Phys. Rev. Lett.*, 98:086401, Feb 2007.

[25] Insook Yi, Yoshiaki Sugimoto, Ryuji Nishi, and Seizo Morita. Study on topographic images of Sn/Si(111)-($\sqrt{3}\times\sqrt{3}$) R30° surface by non-contact AFM. *Surface Science*, 600(17):3382 – 3387, 2006.

[26] J. M. Carpinelli, H. H. Weitering, M. Bartkowiak, R. Stumpf, and E. W. Plummer. Surface Charge Ordering Transition: α Phase of Sn/Ge(111). *Phys. Rev. Lett.*, 79:2859–2862, Oct 1997.

[27] S.T. Jemander, N. Lin, H.M. Zhang, R.I.G. Uhrberg, and G.V. Hansson. An STM study of the surface defects of the ($\sqrt{3}\times\sqrt{3}$)-Sn/Si(111) surface. *Surface Science*, 475(1):181 – 193, 2001.

[28] R. I. G. Uhrberg, H. M. Zhang, T. Balasubramanian, S. T. Jemander, N. Lin, and G. V. Hansson. Electronic structure of Sn/Si(111) $\sqrt{3}\times\sqrt{3}$: Indications of a low-temperature phase. *Phys. Rev. B*, 62:8082–8086, Sep 2000.

[29] L Ottaviano, G Profeta, A Continenza, S Santucci, AJ Freeman, and S Modesti. Defect-induced perturbation on the Sn–Si (111) surface: a voltage-dependent scanning tunneling microscopy study. *Surface science*, 464(2-3):57–67, 2000.

[30] PEJ Eriksson, JR Osiecki, Kazuyuki Sakamoto, and RIG Uhrberg. Atomic and electronic structures of the ordered 2 3× 2 3 and molten 1× 1 phase on the Si (111): Sn surface. *Physical Review B*, 81(23):235410, 2010.

[31] C. Törnevik, M. Hammar, N. G. Nilsson, and S. A. Flodström. Epitaxial growth of Sn on Si(111): A direct atomic-structure determination of the Si(111)-$(2\sqrt{3}\times 2\sqrt{3})$ R 30° reconstructed surface. *Phys. Rev. B*, 44:13144–13147, Dec 1991.

[32] JJ Lander and J Morrison. Surface reactions of silicon with aluminum and with indium. *Surface Science*, 2:553–565, 1964.

[33] J Kraft, MG Ramsey, and FP Netzer. Surface reconstructions of In on Si (111). *Physical Review B*, 55(8):5384, 1997.

[34] Han Woong Yeom, S Takeda, E Rotenberg, I Matsuda, K Horikoshi, J Schaefer, CM Lee, SD Kevan, T Ohta, T Nagao, et al. Instability and charge density wave of metallic quantum chains on a silicon surface. *Physical review letters*, 82(24):4898, 1999.

[35] SJ Park, HW Yeom, JR Ahn, and I-W Lyo. Atomic-scale phase coexistence and fluctuation at the quasi-one-dimensional metal-insulator transition. *Physical review letters*, 95(12):126102, 2005.

[36] Dimitrios Vlachos, Mattheos Kamaratos, Stylianos D Foulias, Federica Bondino, Elena Magnano, and Marco Malvestuto. Indium Growth on Reconstructed Si (111) $\sqrt{3}\times\sqrt{3}$ and 4× 1 In Surfaces. *The Journal of Physical Chemistry C*, 114(41):17693–17702, 2010.

[37] Peter Matvija. Interaction of adsorbates with passivated Si surfaces studied by STM. Master's thesis, Charles University, 2012.

[38] Arieh Aviram and Mark A Ratner. Molecular rectifiers. *Chemical Physics Letters*, 29(2):277–283, 1974.

[39] Dong Xiang, Xiaolong Wang, Chuancheng Jia, Takhee Lee, and Xuefeng Guo. Molecular-scale electronics: from concept to function. *Chemical reviews*, 116(7):4318–4440, 2016.

[40] Jianzhuang Jiang. *Functional phthalocyanine molecular materials*, volume 135. Springer, 2010.

[41] Juergen Braun, Martin Koecher, Martin Schlabach, Bernd Wehrle, Han-Heinrich Limbach, and Emanuel Vogel. NMR study of the tautomerism of porphyrin including the kinetic HH/HD/DD isotope effects in the liquid and the solid state. *Journal of the American Chemical Society*, 116(15):6593–6604, 1994.

[42] Gianlorenzo Bussetti, Marcello Campione, Michele Riva, Andrea Picone, Luisa Raimondo, Lorenzo Ferraro, Conor Hogan, Maurizia Palummo, Alberto Brambilla, Marco Finazzi, et al. Stable alignment of tautomers at room temperature in porphyrin 2d layers. *Advanced Functional Materials*, 24(7):958–963, 2014.

[43] Bernd Wehrle and Hans-heinrich Limbach. NMR study of environment modulated proton tautomerism in crystalline and amorphous phthalocyanine. *Chemical physics*, 136(2):223–247, 1989.

[44] Tatyana Strenalyuk, Svein Samdal, and Hans Vidar Volden. Molecular structure of the trans and cis isomers of metal-free phthalocyanine studied by gas-phase electron diffraction and high-level quantum chemical calculations: NH tautomerization and calculated vibrational frequencies. *The Journal of Physical Chemistry A*, 112(21):4853–4860, 2008.

[45] T Ikeda, R Iino, and H Noji. Real-time fluorescence visualization of slow tautomerization of single free-base phthalocyanines under ambient conditions. *Chemical Communications*, 50(67):9443–9446, 2014.

[46] Jacques Simon and J-J Andre. *Molecular semiconductors: photoelectrical properties and solar cells*. Springer Science & Business Media, 2012.

[47] Mihaela Gorgoi. *Electronic Properties of Phthalocyanines Deposited on H-Si(111)*. PhD thesis, Technische Universität Chemnitz, 2005.

[48] E Orti, JL Bredas, and C Clarisse. Electronic structure of phthalocyanines: theoretical investigation of the optical properties of phthalocyanine monomers, dimers, and crystals. *The Journal of chemical physics*, 92(2):1228–1235, 1990.

[49] Yasutaka Kuzumoto, Hirotaka Matsuyama, and Masatoshi Kitamura. Partially fluorinated copper phthalocyanine toward band engineering for high-efficiency organic photovoltaics. *Japanese Journal of Applied Physics*, 53(1S):01AB03, 2013.

[50] P. Matvija, F. Rozbořil, P. Sobotík, I. Ošťádal, and P. Kocán. Pair Correlation Function of a 2D Molecular Gas Directly Visualized by Scanning Tunneling Microscopy. *J. Phys. Chem. Lett.*, 8(17):4268–4272, 2017.

[51] Nicolas Papageorgiou, Eric Salomon, Thierry Angot, Jean-Marc Layet, Luca Giovanelli, and Guy Le Lay. Physics of ultra-thin phthalocyanine films on semiconductors. *Progress in surface science*, 77(5-8):139–170, 2004.

[52] MC Hersam, NP Guisinger, and JW Lyding. Isolating, imaging, and electrically characterizing individual organic molecules on the Si (100) surface with the scanning tunneling microscope. *Journal of Vacuum Science & Technology A: Vacuum, Surfaces, and Films*, 18(4):1349–1353, 2000.

[53] Younes Makoudi, Judicaël Jeannoutot, Frank Palmino, Frédéric Chérioux, Guillaume Copie, Christophe Krzeminski, Fabrizio Cleri, and Bruno Grandidier. Supramolecular self-assembly on the B-Si(111)-$\sqrt{3}\times\sqrt{3}$) R 30° surface: From single molecules to multicomponent networks. *Surface Science Reports*, 72(4):316 – 349, 2017.

[54] Dongchul Shin, Zheng Wei, Hyungjoon Shim, and Geunseop Lee. Adsorption and ordering of PTCDA on various reconstruction surfaces of In/Si (1 1 1). *Applied Surface Science*, 372:87–92, 2016.

[55] Nicoleta Nicoara, Zheng Wei, and José M Gímez-Rodríguez. One-Dimensional Growth of PTCDA Molecular Rows on Si (111)-($2\sqrt{3}\times 2\sqrt{3}$) R30°-Sn Surfaces. *The Journal of Physical Chemistry C*, 113(33):14935–14940, 2009.

[56] HM Zhang and LSO Johansson. STM study of PTCDA on Sn/Si (111)-$2\sqrt{3}\times 2\sqrt{3}$. *The Journal of chemical physics*, 144(12):124701, 2016.

[57] H. M. Zhang, J. B. Gustafsson, and L. S. O. Johansson. Electronic structure of PTCDA on Sn/Si(111)-$\sqrt{3}\times\sqrt{3}$. *Phys. Rev. B*, 84:205420, Nov 2011.

[58] D.V. Gruznev, A.V. Matetskiy, A.V. Zotov, A.A. Saranin, J.P. Chou, C.M. Wei, and Y.L. Wang. Interplay between adsorbed C60 fullerenes and point defects on a Si(111)$\sqrt{3}\times\sqrt{3}$–In reconstructed surface. *Surface Science*, 605(23):2050 – 2054, 2011.

[59] Physical properties of Fullerenes. `https://www.sesres.com/physical-properties/`. Accessed: 2017-04-20.

[60] Yongfeng Wang, Jörg Kröger, Richard Berndt, and Werner A Hofer. Pushing and pulling a Sn ion through an adsorbed phthalocyanine molecule. *Journal of the American Chemical Society*, 131(10):3639–3643, 2009.

[61] Christophe Nacci, K Kanisawa, and S Fölsch. Reversible switching of single tin phthalocyanine molecules on the InAs (111) A surface. *Journal of Physics: Condensed Matter*, 24(39):394004, 2012.

[62] Jialin Zhang, Zhunzhun Wang, Tianchao Niu, Zhenyu Li, and Wei Chen. Single molecule tunneling spectroscopy investigation of reversibly switched dipolar vanadyl phthalocyanine on graphite. *Applied Physics Letters*, 104(11):113506, 2014.

[63] Yu Li Huang, Yunhao Lu, Tian Chao Niu, Han Huang, Satoshi Kera, Nobuo Ueno, Andrew Thye Shen Wee, and Wei Chen. Reversible single-molecule switching in an ordered monolayer molecular dipole array. *Small*, 8(9):1423–1428, 2012.

[64] Takashi Kumagai, Felix Hanke, Sylwester Gawinkowski, John Sharp, Konstantinos Kotsis, Jacek Waluk, Mats Persson, and Leonhard Grill. Thermally and vibrationally induced tautomerization of single porphycene molecules on a Cu (110) surface. *Physical review letters*, 111(24):246101, 2013.

[65] Karel Majer, Petr Zimmermann, and Pavel Sobotík. Fluctuations of phthalocyanine molecules on passivated silicon surfaces studied by STM at room temperature. unpublished results.

[66] Peter Matvija. *Influence of Si surface passivation on growth and ordering of nanostructures.* PhD thesis, Charles University, 2017.

[67] Pavel Kocán. *Study of Heteroepitaxial Growth on Reconstructed Si Surfaces.* PhD thesis, Charles University, 2004.

[68] David Nečas and Petr Klapetek. Gwyddion: an open-source software for SPM data analysis. *Central European Journal of Physics*, 10:181–188, 2012.

[69] M Prietsch, A Samsavar, and R Ludeke. Structural and electronic properties of the Bi/GaP (110) interface. *Physical Review B*, 43(14):11850, 1991.

[70] Peter Matvija, Filip Rozbořil, Pavel Sobotík, Ivan Ošt'ádal, Barbara Pieczyrak, Leszek Jurczyszyn, and Pavel Kocán. Electric-field-controlled phase transition in a 2D molecular layer. *Scientific reports*, 7(1):7357, 2017.

List of Figures

List of Tables

List of Abbreviations

AC alternating current

ARUPS Angle-resolved ultraviolet photo electron spectroscopy

CDF cumulative density function

CuPc copper phthalocyanine

DAS dimer-adatom-stacking-fault

DB dangling bond

DFT Density functional theory

F_8CuPc copper octafluorophthalocyanine

F_{16}CuPc copper hexadecafluorophthalocyanine

H_2Pc metal-free phthalocyanine

HOMO highest occupied molecular orbital electron spectroscopy

LDOS local density of states

LUMO lowest unoccupied molecular orbital

LEED Low energy electron diffraction

ML monolayer

MPcs metalllophthalocyanines

NMR Nuclear magnetic resonance (spectroscopy)

PID proportional-integral–derivative

PTCDA perylenetetracarboxylic dianhydride

RHEED Reflection high-energy electron diffraction

RT room temperature

STM Scanning tunneling microscopy/Scanning tunneling microscope

STS Scanning tunneling spectroscopy

UHV ultra-high vacuum